Hindawi Publishing Corporation
EURASIP Journal on Wireless Communications and Networking
Volume 2008, Article ID 391025, 16 pages
doi:10.1155/2008/391025

Research Article

Analysis and Compensation of Transmitter and Receiver I/Q Imbalances in Space-Time Coded Multiantenna OFDM Systems

Yaning Zou, Mikko Valkama, and Markku Renfors

Institute of Communications Engineering, Tampere University of Technology, P.O.Box 553, 33101 Tampere, Finland

Correspondence should be addressed to Yaning Zou, yaning.zou@tut.fi

Received 30 April 2007; Revised 27 August 2007; Accepted 30 October 2007

Recommended by Hikmet Sari

The combination of orthogonal frequency division multiplexing (OFDM) and multiple-input multiple-output (MIMO) techniques has been widely considered as the most promising approach for building future wireless transmission systems. The use of multiple antennas poses then big restrictions on the size and cost of individual radio transmitters and receivers, to keep the overall transceiver implementation feasible. This results in various imperfections in the analog radio front ends. One good example is the so-called I/Q imbalance problem related to the amplitude and phase matching of the transceiver I and Q chains. This paper studies the performance of space-time coded (STC) multiantenna OFDM systems under I/Q imbalance, covering both the transmitter and the receiver sides of the link. The challenging case of frequency-selective I/Q imbalances is assumed, being an essential ingredient in future wideband wireless systems. As a practical example, the Alamouti space-time coded OFDM system with two transmit and M receive antennas is examined in detail and a closed-form solution for the resulting signal-to-interference ratio (SIR) at the detector input due to I/Q imbalance is derived. This offers a valuable analytical tool for assessing the I/Q imbalance effects in any STC-OFDM system, without lengthy data or system simulations. In addition, the impact of I/Q imbalances on the channel estimation in the STC-OFDM context is also analyzed analytically. Furthermore, based on the derived signal models, a practical pilot-based I/Q imbalance compensation scheme is also proposed, being able to jointly mitigate the effects of frequency-selective I/Q imbalances as well as channel estimation errors. The performance of the compensator is analyzed using extensive computer simulations, and it is shown to virtually reach the perfectly matched reference system performance with low pilot overhead.

1. INTRODUCTION

The limited spectral resources and the fast rising demands on system throughput and network capacity are generally considered as the main challenge and also the driving force in the development and evolution of future wireless communication systems. It is crucial to find means of improving system performance in terms of the overall spectral efficiency as well as the individual link quality [1, 2]. One of the most promising methods for increasing the data rates is to generate parallel "data pipes" by utilizing multiple transmit and receive antennas together with the multipath propagation phenomenon of the physical radio channels. This leads to the so-called multiple-input multiple-output (MIMO) system concepts [1, 3, 4]. The constructed space-time-frequency "matrix" enables a number of ways to efficiently improve throughput and system capacity. Another important ingredient in multiantenna developments is the ability to improve the link quality through the obtained spatial diversity [3–5]. This is already part of the current 3G UMTS standard [6], under the acronym STTD (space-time transmit diversity).

In addition to spatial multiplexing, wider signaling bandwidths are also taken into use to achieve higher absolute data rates. As an example, overall bandwidths in the order of 5–20 MHz are specified in 3G long-term evolution (LTE) [7]. But wideband channels are much more difficult to be dealt with than their narrowband counterparts. One efficient solution for coping with and taking use of the wideband radio channels is to use OFDM [1, 2]. By converting the overall frequency-selective channel into a collection of parallel frequency-flat subchannels, OFDM modulation combined with proper coding can take advantage of the frequency diversity in multipath environments. Therefore, when targeting for spectral efficiencies in the order of 10 bits/s/Hz and absolute data rates of 100 Mbits/s and above in the emerging wireless systems [1, 2], the combination of MIMO and

OFDM has generally drawn wide attention and theoretic research interest in both communication theoretic as well as signal processing research communities.

While OFDM-based multiantenna transmission techniques have received lots of research interest at communication theoretic research community and baseband signal processing levels, the radio implementation aspects and their implications on the system performance and design have only recently started to receive some interest. With multiple transmit and/or receive antennas, also multiple radio implementations are needed, and the limited overall implementation resources cause then big restrictions on the size and cost of individual radios. Thus in this context, rather simple radio frequency (RF) front-ends, like the direct-conversion and low-IF radios [8, 9], are likely to be deployed. As a result, the so-called "dirty-RF" paradigm referring to the effects of various nonidealities of the individual transmitter and receiver analog front-ends becomes one essential ingredient [10, 11]. In general, the nature and role of these RF impairments depend strongly on the applied radio architecture as well as on the used communication waveforms. In multiantenna systems utilizing wideband OFDM waveforms, together with high-order subcarrier modulation and spatial signal processing, the role of the RF impairments is likely to be more critical than in many traditional existing wireless systems. This is indicated by the preliminary studies of the field [12–18].

One important practical RF impairment, being also the topic of this paper, is the so-called I/Q imbalance phenomenon [8–11, 19], stemming from the unavoidable differences in the relative amplitudes and phases of the physical analog I and Q signal paths. The basic I/Q imbalance effect, assuming *frequency-independent* imbalances within the whole system band, has been recently addressed in the MIMO context in [12–18, 20–23]. Also, some compensation techniques for mitigating *frequency-independent* I/Q imbalances have been proposed, focusing mainly on receiver imbalances. In practice, however, with bandwidths in the order of several or tens of MHz, the simplifying assumption of frequency-independent I/Q imbalance is unrealistic, and thus it is dropped in this paper. The frequency-dependent case is also assumed recently in [24], in which a combination of pilot-based and decision-directed processing techniques is utilized. Notice, however, that the space-time coding element is not addressed in [24], but a direct spatial multiplexing case is assumed.

The starting point for this paper is the earlier work by the authors in [15, 16], which considers space-time coded single-carrier systems and assumes frequency-independent I/Q imbalance, and in [17] in which the performance of STC-OFDM system with frequency-independent imbalances is studied. In this paper, we address the considerably more challenging case of analyzing and compensating for the impacts of frequency-selective I/Q imbalances in space-time coded multiantenna OFDM systems. Imbalances are assumed on both the transmitter as well as the receiver sides of the link, which is the case also in practice. More specifically, as a practical example system, $2 \times M$ Alamouti transmit diversity scheme [5] applied at OFDM subcarrier level is assumed, and the direct-conversion radio architecture is used in the individual front-end implementations. Overall system model is developed from the transmitted data stream to the receiver diversity combiner output, including the effects of transmitter and receiver I/Q imbalances as well as arbitrary multipath channels in between. Stemming from the derived signal models, analytical *system-level* performance figures in terms of the subcarrierwise signal-to-interference ratio (SIR) at the output of the receiver combining stage are derived, being further verified using computer simulations, to assess the exact imbalance effect analytically. This gives a valuable analytical tool for the system and transceiver designers for analyzing the imbalance effects without lengthy system simulations, and thus it forms a solid theoretical basis for fully appreciating the imbalance effects in any STC-OFDM context. Based on the analysis, with realistic frequency-selective I/Q imbalances and practical frequency-selective multipath channels, the resulting SIRs can easily range down to 20 dB or so, even with very high-quality *individual radios*. The SIR is also heavily subcarrier-specific with differences even in the order of 5 dB or so, assuming practical imbalance values and multipath profiles. The analytical derivations also include the effects of *imperfect channel knowledge* or channel estimation errors, due to I/Q imbalance and additive channel noise, which degrades the system performance further. This aspect is also included in the analysis, being formalized in terms of the so-called channel-to-noise ratio (CNR) measuring the quality of the channel estimates. Furthermore, based on the developed signal models for the overall system, together with properly allocated pilot data, a novel baseband digital signal processing approach is proposed to jointly mitigate or compensate for the dominant I/Q imbalance effects together with the effects of channel estimation errors on the receiver side of the link. Comprehensive computer simulations are used to illustrate the validity and accuracy of the SIR and CNR analyses, on one side, and the good compensation performance of the proposed mitigation technique on the other side. This gives strong confidence on being able to reduce the considered RF impairment effects to acceptable levels in future digital radio evolutions.

The rest of the paper is organized as follows. Section 2 presents the essential frequency-selective I/Q impairment models for the individual transmitter and receiver front-ends, together with the overall subcarrierwise system model for the STC-OFDM transmission under the imbalances. Based on the derived models, the level of signal distortion due to the imbalances is analyzed in Section 3 in terms of signal-to-interference ratio (SIR), assuming arbitrary frequency-selective multipath radio channels linking the transmitters and the receivers. Section 4, in turn, proposes an effective pilot-based I/Q impairment mitigation technique, being able to handle the challenging case of frequency-selective I/Q imbalances. The effect of I/Q imbalances and noise on the channel estimation quality is also addressed in Section 4, in terms of the so-called channel-to-noise ratio (CNR) analysis. Furthermore, it is shown that the proposed I/Q imbalance compensator is, by design, able to mitigate the effects of channel estimation errors as well, with zero additional cost. Section 5 focuses on numerical illustrations and performance simulations, validating the analysis

results of Sections 3 and 4 as well as demonstrating the efficiency and good performance of the proposed compensation technique. Finally, conclusions are drawn in Section 6.

2. I/Q SIGNAL AND SYSTEM MODELS

2.1. Mathematical notations and preliminaries

Throughout the text, unless otherwise mentioned explicitly, all the signals are assumed to be complex-valued, wide-sense stationary (WSS) random signals with zero mean. The so-called I/Q notation of the form $x = x_I + jx_Q$ is commonly deployed for any complex-valued quantity x, where x_I and x_Q denote the corresponding real and imaginary parts, that is, $\mathrm{Re}[x] = x_I$ and $\mathrm{Im}[x] = x_Q$. Statistical expectation and complex conjugation are denoted by $E[\cdot]$ and $(\cdot)^*$, respectively. We also assume that the complex random signals and random quantities at hand, under perfect I/Q balance, are circular (see, e.g., [25]), meaning basically that the I and Q components are uncorrelated and have equal variance. For a circular random signal $x(t)$, this also implies that $E[x^2(t)] = E[x(t)(x^*(t))^*] = 0$, which simplifies the performance analysis. Convolution between two time functions is denoted by $x(t) * y(t)$, and Dirac impulse is denoted by $\delta(t)$.

2.2. General frequency-dependent I/Q mismatch models

The amplitude and phase mismatches between the transceiver I and Q signal branches stem from the relative differences between all the analog components of the I/Q front-end [8–11, 19]. On the transmitter side, this includes the actual I/Q upconversion stage as well as the I and Q branch D/A converters and lowpass filters. On the receiver side, on the other hand, the I/Q downconversion as well as the I- and Q branch filtering, amplification, sampling, and A/D stages contribute to the effective I/Q imbalance. In the wideband system context, the overall effective I/Q imbalances vary as a function of frequency within the system band [8, 19], which should also be reflected in imbalance modeling as well as imbalance compensation. Here, we first model the *frequency-independent* I/Q imbalances due to the quadrature (I/Q) mixers as

$$\begin{aligned} x_{\mathrm{LO}}^{\mathrm{TX}}(t) &= \cos(\omega_{\mathrm{LO}}t) + jg_{\mathrm{TX}}\sin(\omega_{\mathrm{LO}}t + \phi_{\mathrm{TX}}), \\ x_{\mathrm{LO}}^{\mathrm{RX}}(t) &= \cos(\omega_{\mathrm{LO}}t) - jg_{\mathrm{RX}}\sin(\omega_{\mathrm{LO}}t + \phi_{\mathrm{RX}}), \end{aligned} \tag{1}$$

where $\omega_{\mathrm{LO}} = 2\pi f_{\mathrm{LO}}$, and $\{g_{\mathrm{TX}}, \phi_{\mathrm{TX}}\}$ and $\{g_{\mathrm{RX}}, \phi_{\mathrm{RX}}\}$ represent the amplitude and phase imbalances of the transmitter (TX) and the receiver (RX) quadrature mixing stages, respectively. This is the standard approach in the literature (see, e.g., [10, 20, 22], and the references therein). Then, the *frequency-selective* branch mismatches are also taken into account, in terms of branch filters $h_{\mathrm{TX}}(t)$ and $h_{\mathrm{RX}}(t)$, which represent the I and Q branch *frequency-response differences*, in the transmitter and receiver, respectively. Then, if $z(t) = z_I(t) + jz_Q(t)$ denotes the ideal (perfect I/Q balance) complex baseband equivalent signal, the overall baseband equivalent I/Q imbalance models for individual transmitters and receivers appear as

$$\begin{aligned} z_{\mathrm{TX}}(t) &= g_{1,\mathrm{TX}}(t) * z(t) + g_{2,\mathrm{TX}}(t) * z^*(t), \\ z_{\mathrm{RX}}(t) &= g_{1,\mathrm{RX}}(t) * z(t) + g_{2,\mathrm{RX}}(t) * z^*(t), \end{aligned} \tag{2}$$

where the effective impulse responses $g_{1,\mathrm{TX}}(t)$, $g_{2,\mathrm{TX}}(t)$, $g_{1,\mathrm{RX}}(t)$, and $g_{2,\mathrm{RX}}(t)$ are depending on the actual imbalance properties as $g_{1,\mathrm{TX}}(t) = (\delta(t) + h_{\mathrm{TX}}(t)g_{\mathrm{TX}}e^{j\phi_{\mathrm{TX}}})/2$, $g_{2,\mathrm{TX}}(t) = (\delta(t) - h_{\mathrm{TX}}(t)g_{\mathrm{TX}}e^{j\phi_{\mathrm{TX}}})/2$, $g_{1,\mathrm{RX}}(t) = (\delta(t) + h_{\mathrm{RX}}(t)g_{\mathrm{RX}}e^{-j\phi_{\mathrm{RX}}})/2$, and $g_{2,\mathrm{RX}}(t) = (\delta(t) - h_{\mathrm{RX}}(t)g_{\mathrm{RX}}e^{j\phi_{\mathrm{RX}}})/2$. Notice that the typical frequency-independent (instantaneous) I/Q imbalance models of the form $z_{\mathrm{TX}}(t) = K_{1,\mathrm{TX}}z(t) + K_{2,\mathrm{TX}}z^*(t)$ and $z_{\mathrm{RX}}(t) = K_{1,\mathrm{RX}}z(t) + K_{2,\mathrm{RX}}z^*(t)$ are obtained as special cases of (2) when $h_{\mathrm{TX}}(t) = \delta(t)$ and $h_{\mathrm{RX}}(t) = \delta(t)$.

Based on the models in (2), when viewed in frequency domain, the distortion due to I/Q imbalance (the conjugate signal terms in (2)) corresponds to *mirror-frequency interference* whose strength varies as a function of frequency. This can be seen by taking Fourier transforms of (2), yielding

$$\begin{aligned} Z_{\mathrm{TX}}(f) &= G_{1,\mathrm{TX}}(f)Z(f) + G_{2,\mathrm{TX}}(f)Z^*(-f), \\ Z_{\mathrm{RX}}(f) &= G_{1,\mathrm{RX}}(f)Z(f) + G_{2,\mathrm{RX}}(f)Z^*(-f), \end{aligned} \tag{3}$$

in which the transfer functions $G_{1,\mathrm{TX}}(f) = (1 + H_{\mathrm{TX}}(f)g_{\mathrm{TX}}e^{j\phi_{\mathrm{TX}}})/2$, $G_{2,\mathrm{TX}}(f) = (1 - H_{\mathrm{TX}}(f)g_{\mathrm{TX}}e^{j\phi_{\mathrm{TX}}})/2$, $G_{1,\mathrm{RX}}(f) = (1 + H_{\mathrm{RX}}(f)g_{\mathrm{RX}}e^{-j\phi_{\mathrm{RX}}})/2$, $G_{2,\mathrm{RX}}(f) = (1 - H_{\mathrm{RX}}(f)g_{\mathrm{RX}}e^{j\phi_{\mathrm{RX}}})/2$. Thus, the corresponding mirror-frequency attenuations or image rejection ratios (IRRs) of the individual front-ends are then given by

$$\begin{aligned} L_{\mathrm{TX}}(f) &= \frac{|G_{1,\mathrm{TX}}(f)|^2}{|G_{2,\mathrm{TX}}(f)|^2}, \\ L_{\mathrm{RX}}(f) &= \frac{|G_{1,\mathrm{RX}}(f)|^2}{|G_{2,\mathrm{RX}}(f)|^2}. \end{aligned} \tag{4}$$

With practical analog front-end electronics, these mirror-frequency attenuations are in the range of 25–40 dB [8, 9] and vary as a function of frequency when bandwidths in the order of several MHz are considered [8, 19]. This is illustrated in Figure 1 which shows the *measured mirror-frequency attenuation* characteristics, obtained in comprehensive laboratory test measurements of state-of-the-art wireless receiver RF-IC operating at 2 GHz. Clearly, for bandwidths in the order of 1–10 MHz, the mirror-frequency attenuation (and thus the effective I/Q imbalances) indeed depend on frequency.

2.3. Space-time coded multiantenna OFDM under transmitter and receiver I/Q mismatches

A multiantenna space-time coded transmission system utilizing $2 \times M$ Alamouti transmit diversity scheme [5] combined with OFDM modulation [3] is considered here. As shown in Figure 2, with $M = 1$ receiver as a simple practical example, space-time coding is applied separately for each subcarrier data stream and then transmitted using two parallel

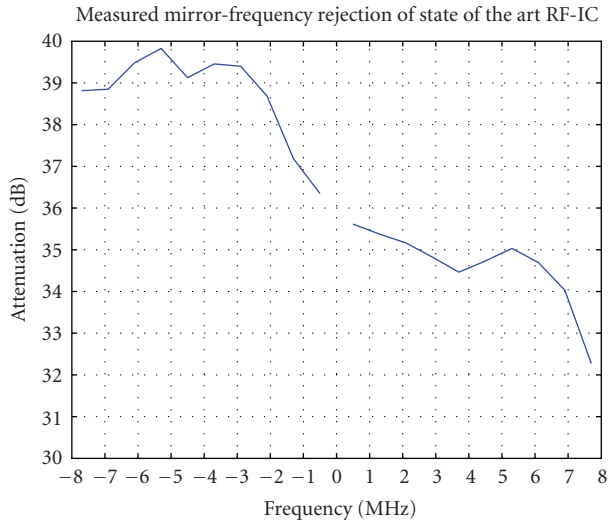

Figure 1: Measured mirror-frequency attenuation of state-of-the-art I/Q receiver RF-IC operating at 2 GHz RF. The x-axis refers to frequencies of the downconverted complex (I/Q) signal, or equivalently, to the frequencies around the LO frequency at RF.

OFDM transmitters. On the receiver side, diversity combining is then applied over two consecutive OFDM symbol intervals.

Now let $s_1(k)$ and $s_2(k)$ represent the two consecutive data samples to be transmitted over the kth subcarrier. Assuming that the guard interval (GI) implemented as a cyclic prefix (CP) is longer than the multipath channel delay spread, which is a typical assumption in any CP-OFDM system, the corresponding samples at the output of the mth receiver FFT stage (kth bin) after CP removal are given by [3]

$$\begin{aligned} x_{1,m}(k) &= H_{1,m}(k)s_1(k) + H_{2,m}(k)s_2(k), \\ x_{2,m}(k) &= -H_{1,m}(k)s_2^*(k) + H_{2,m}(k)s_1^*(k). \end{aligned} \tag{5}$$

Here, $H_{1,m}(k)$ and $H_{2,m}(k)$ denote the baseband equivalent radio channel frequency responses (TX(1)→RX(m) and TX(2)→RX(m)) at subcarrier k, between the two transmitters and mth receiver, and the additive noise is ignored for simplicity. Also, perfect I/Q balance in the transmitters and receivers is assumed for a while. Then, assuming further that perfect channel knowledge is available at the receivers, diversity combining is carried out over two consecutive symbol intervals as [3, 5]

$$\begin{aligned} y_1(k) &= \sum_{m=1}^{M} \left(H_{1,m}^*(k)x_{1,m}(k) + H_{2,m}(k)x_{2,m}^*(k)\right) \\ &= \sum_{m=1}^{M} \left(\left|H_{1,m}(k)\right|^2 + \left|H_{2,m}(k)\right|^2\right)s_1(k), \\ y_2(k) &= \sum_{m=1}^{M} \left(H_{2,m}^*(k)x_{1,m}(k) - H_{1,m}(k)x_{2,m}^*(k)\right) \\ &= \sum_{m=1}^{M} \left(\left|H_{1,m}(k)\right|^2 + \left|H_{2,m}(k)\right|^2\right)s_2(k). \end{aligned} \tag{6}$$

As it is obvious, this yields diversity gain over the individual fading links. For amplitude modulated data, proper scaling by $1/\sum_{m=1}^{M}(|H_{1,m}(k)|^2 + |H_{2,m}(k)|^2)$ is of course needed. Notice that in addition to the cyclic prefix assumption, no further assumptions are made on the frequency selectivity of the radio channels.

The overall data transmission at any specific subcarrier k is described by (5) and (6), assuming ideal radio transmitters and receivers. Incorporating next the general TX and RX I/Q impairment models in (3) into the considered STC-OFDM system setup, the corresponding observations at the output of the diversity combining stage at subcarrier k can be shown to be of the form

$$\begin{aligned} y_1(k) &= a(k)s_1(k) + b(k)s_1^*(-k) + c(k)s_2(k) + d(k)s_2^*(-k), \\ y_2(k) &= a^*(k)s_2(k) + b^*(k)s_2^*(-k) - c^*(k)s_1(k) - d^*(k)s_1^*(-k). \end{aligned} \tag{7}$$

Here, it is assumed that the active subcarriers are located symmetrically around the zero frequency. With this assumption, (7) follows directly by combining (3), (5), and (6). The exact expressions for the imbalanced system coefficients $a(k)$, $b(k)$, $c(k)$, and $d(k)$, as functions of the individual transmitter and receiver imbalance properties ($G_{1,\mathrm{TX}(n)}(k)$, $G_{2,\mathrm{TX}(n)}(k)$, $n = 1, 2$ and $G_{1,\mathrm{RX}(m)}(k)$, $G_{2,\mathrm{RX}(m)}(k)$, $m = 1, 2, \ldots, M$), are given by

$$\begin{aligned} a(k) = \sum_{m=1}^{M} &\left(\left|H_{1,m}(k)\right|^2 G_{1,\mathrm{RX}(m)}(k)G_{1,\mathrm{TX}(1)}(k)\right. \\ &+ H_{1,m}^*(k)H_{1,m}^*(-k)G_{2,\mathrm{RX}(m)}(k)G_{2,\mathrm{TX}(1)}^*(-k) \\ &+ \left|H_{2,m}(k)\right|^2 G_{1,\mathrm{RX}(m)}^*(k)G_{1,\mathrm{TX}(2)}^*(k) \\ &\left.+ H_{2,m}(k)H_{2,m}(-k)G_{2,\mathrm{RX}(m)}^*(k)G_{2,\mathrm{TX}(2)}(-k)\right), \\ b(k) = \sum_{m=1}^{M} &\left(\left|H_{1,m}(k)\right|^2 G_{1,\mathrm{RX}(m)}(k)G_{2,\mathrm{TX}(1)}(k)\right. \\ &+ H_{1,m}^*(k)H_{1,m}^*(-k)G_{2,\mathrm{RX}(m)}(k)G_{1,\mathrm{TX}(1)}^*(-k) \\ &+ \left|H_{2,m}(k)\right|^2 G_{1,\mathrm{RX}(m)}^*(k)G_{2,\mathrm{TX}(2)}^*(k) \\ &\left.+ H_{2,m}(k)H_{2,m}(-k)G_{2,\mathrm{RX}(m)}^*(k)G_{1,\mathrm{TX}(2)}(-k)\right), \\ c(k) = \sum_{m=1}^{M} &\left(H_{1,m}^*(k)H_{2,m}(k)G_{1,\mathrm{RX}(m)}(k)G_{1,\mathrm{TX}(2)}(k)\right. \\ &+ H_{1,m}^*(k)H_{2,m}^*(-k)G_{2,\mathrm{RX}(m)}(k)G_{2,\mathrm{TX}(2)}^*(-k) \\ &- H_{1,m}^*(k)H_{2,m}(k)G_{1,\mathrm{RX}(m)}^*(k)G_{1,\mathrm{TX}(1)}^*(k) \\ &\left.- H_{1,m}(-k)H_{2,m}(k)G_{2,\mathrm{RX}(m)}^*(k)G_{2,\mathrm{TX}(1)}(-k)\right), \\ d(k) = \sum_{m=1}^{M} &\left(H_{1,m}^*(k)H_{2,m}(k)G_{1,\mathrm{RX}(m)}(k)G_{2,\mathrm{TX}(2)}(k)\right. \\ &+ H_{1,m}^*(k)H_{2,m}^*(-k)G_{2,\mathrm{RX}(m)}(k)G_{1,\mathrm{TX}(2)}^*(-k) \\ &- H_{1,m}^*(k)H_{2,m}(k)G_{1,\mathrm{RX}(m)}^*(k)G_{2,\mathrm{TX}(1)}^*(k) \\ &\left.- H_{1,m}(-k)H_{2,m}(k)G_{2,\mathrm{RX}(m)}^*(k)G_{1,\mathrm{TX}(1)}(-k)\right). \end{aligned} \tag{8}$$

In general, based on (7), the observations at any individual subcarrier k are interfered by the conjugate of the data at the corresponding mirror carrier $-k$ as well as by the other data symbol within the STC block at subcarriers k and $-k$. Closer

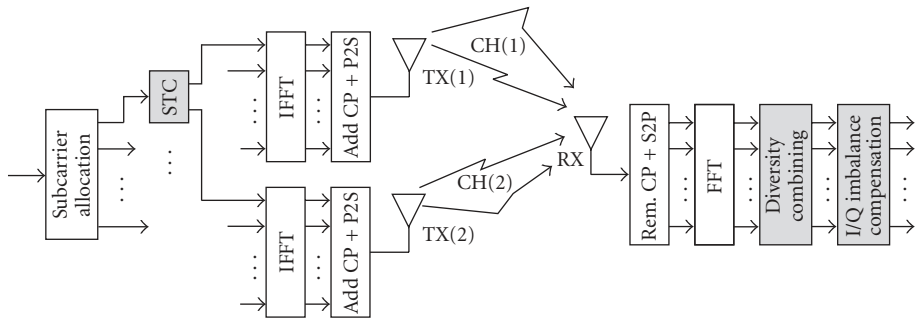

Figure 2: Space-time coded (STC) multiantenna (2×1) OFDM system with subcarrierwise STC. Diversity combining and I/Q imbalance compensation are also carried out on a subcarrier-per-subcarrier basis after receiver FFT.

comparison of the above system model in (7) and (8) with its single-carrier counterpart in [15, 16] reveals some further differences. Assuming independent subcarrier data streams, the combiner outputs here appear as weighted linear combinations of 4 independent data symbols, while in the corresponding single-carrier system, there are only two independent data symbols and their own complex conjugates (see [15] for more details). This has rather big impact on the distribution of the overall interference, and thus it is important when carrying out the statistical interference analysis in the continuation. Another difference lies in the structure of the coefficients $a(k)$, $b(k)$, $c(k)$, and $d(k)$ which, for any subcarrier k, is influenced also by the channel frequency responses and I/Q imbalance properties at the mirror subcarrier $-k$. These aspects will be quantified and demonstrated in detail by both analytical analysis as well as computer simulations in the next sections.

3. SIGNAL-TO-INTERFERENCE RATIO (SIR) ANALYSIS

In what follows, we analyze and quantify the amount of signal distortion due to I/Q imbalance in terms of signal-to-interference ratio (SIR) at the receiver diversity combiner output using the signal models of the previous section. As opposed to the traditional imbalance analysis focusing on *individual radios*, this SIR represents a *system-level performance measure* describing the combined impact of individual imperfections on the overall data transmission (from TX symbols to RX detector input) in the multiantenna STC-OFDM context. Although the distribution of the interference is not exactly Gaussian (being a superposition of three independent data symbols of the used subcarrier constellations), the derived SIR anyway does give clear indication of the relative system performance with different imbalance values and with different radio channel profiles, and thus it forms a useful quality measure in the analysis and design of practical systems. We will also show that the derived SIR values predict the high SNR detection error rate behavior in a very accurate manner. Thus, altogether, the SIR analysis results can be used for system-level impairment analysis without running lengthy data or system simulations.

In the analysis, arbitrary L-tap frequency-selective multipath radio channels are assumed, with the individual taps being modeled as independent circular complex Gaussian random variables with zero mean and power-delay profile $\mathbf{P} = [P(0), P(1), \ldots, P(L-1)]^T$ in which $P(l)$ denotes the power of the lth tap. Based on this, it is easy to show that the channel frequency responses $H_{1,m}(k)$ and $H_{2,m}(k)$ at any subcarrier k are also complex circular Gaussian random variables with zero mean and equal mean power $E[|H_{1,m}(k)|^2] = E[|H_{2,m}(k)|^2] = \sum_{l=0}^{L-1} P(l) = P_H$, $m = 1, 2, \ldots, M$. Then, it follows that for all k, m

(i) $E[H_{1,m}^2(k)] = E[H_{2,m}^2(k)] = 0$,
(ii) $E[H_{1,m}(k)H_{1,m}(-k)] = E[H_{2,m}(k)H_{2,m}(-k)] = 0$,
(iii) $E[H_{1,m}(k)H_{1,m}^*(-k)] = E[H_{2,m}(k)H_{2,m}^*(-k)] = \sum_{l=0}^{L-1} P(l)e^{-j4\pi kl/N}$,
(iv) $E[|H_{1,m}(k)|^4] = E[|H_{2,m}(k)|^4] = 2P_H^2$,
(v) $E[|H_{1,m}(k)|^2 H_{1,m}^2(k)] = E[|H_{2,m}(k)|^2 H_{2,m}^2(k)] = 0$,

which simplifies the following analysis. Now, consider the first combiner output $y_1(k)$ in (7) consisting of the four signal terms. The ideal reference signal (given by (6)) is $\sum_{m=1}^{M}(|H_{1,m}(k)|^2 + |H_{2,m}(k)|^2)s_1(k)$ or $H(k)s_1(k)$, where $H(k) = \sum_{m=1}^{M}(|H_{1,m}(k)|^2 + |H_{2,m}(k)|^2)$. Including amplitude scaling by $1/H(k)$ to both signals, the ideal reference signal becomes simply $H(k)s_1(k)/H(k) = s_1(k)$, and thus the overall system-level interference due to I/Q imbalance is then $[a(k)s_1(k) + b(k)s_1^*(-k) + c(k)s_2(k) + d(k)s_2^*(-k)]/H(k) - s_1(k)$ or $[a(k)/H(k) - 1]s_1(k) + [b(k)/H(k)]s_1^*(-k) + [c(k)/H(k)]s_2(k) + [d(k)/H(k)]s_2^*(-k)$. Then, assuming that the symbols $s_1(k)$, $s_2(k)$, $s_1(-k)$, and $s_2(-k)$ are all equal-variance, uncorrelated, circular complex random variables, and independent of the channel coefficients, the SIR at subcarrier k can be defined as

$$\begin{aligned}\mathrm{SIR}(k) &= \frac{E\left[\left|s_1(k)\right|^2\right]}{E\left[\left|\left(\frac{y_1(k)}{H(k)}\right) - s_1(k)\right|^2\right]} \\ &= 1\Big/\left(E\left[\left|\frac{a(k)}{H(k)} - 1\right|^2\right] + E\left[\left|\frac{b(k)}{H(k)}\right|^2\right] \right. \\ &\qquad \left. + E\left[\left|\frac{c(k)}{H(k)}\right|^2\right] + E\left[\left|\frac{d(k)}{H(k)}\right|^2\right]\right).\end{aligned} \tag{9}$$

Essentially, the SIR in (9) represents the power ratio of the transmit symbol $s_1(k)$ and the undesired signal components

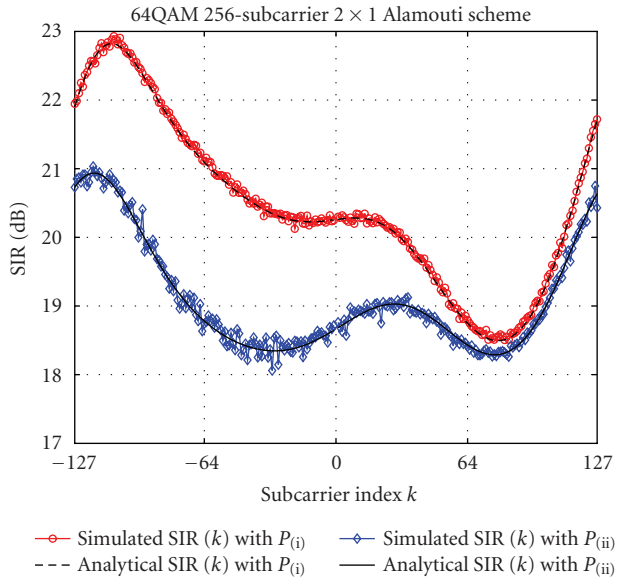

Figure 3: Obtained SIR as a function of the subcarrier index k in a 2×1 STC-OFDM system with realistic frequency-selective I/Q imbalances at both transmitter and receiver analog front-ends, assuming (i) frequency-flat and (ii) arbitrarily frequency-selective radio channels. Both analytical and simulated SIRs are shown.

due to I/Q imbalance at the detector input. Based on (7) and the above assumptions, the SIR in (9) holds also for the second combiner output $y_2(k)$. As will be shown in more detail, this SIR varies as a function of the subcarrier index k and depends on the exact power-delay profile of the radio channels as well as on overall imbalance properties of the transmitters and receivers. Without additional assumptions on the frequency correlation of the radio channels, analytical simplification of the above SIR expression is however somewhat tedious, due to the intercarrier interference between the mirror subcarriers (k and $-k$). Thus, to carry out the analysis further and to get some general understanding on the role of the radio channel type and TX/RX imbalance characteristic on the SIR behavior, we examine next the following two extreme cases: (i) frequency-flat (single-tap) fading channels and (ii) arbitrarily frequency-selective (infinite delay spread) fading channels. In the first case, the channel frequency response values are identical for all the subcarriers, while in the second case, the different subcarriers fade totally independently. At any subcarrier k, this results in a range of SIR values within which the actual SIR in (9) is then confined with practical mobile radio channels. After some rather involved yet relatively straightforward manipulations, these SIR bounds corresponding to the previous cases can be written as

$$\begin{aligned} \mathrm{SIR}_{(\mathrm{i})}(k) &\approx \mathrm{SIR}_{\mathrm{def}}(2, 1, k), \\ \mathrm{SIR}_{(\mathrm{ii})}(k) &\approx \mathrm{SIR}_{\mathrm{def}}(\beta_M, \beta_M, k), \end{aligned} \tag{10}$$

where

Table 1: Values of the parameter β_M with different number of receivers M.

M	1	2	3	4	8
β_M	3	1.66	1.40	1.28	1.133

$$\mathrm{SIR}_{\mathrm{def}}(\alpha_1, \alpha_2, k) = \frac{(2M + 4M^2)}{A(\alpha_1, \alpha_2, k)}, \tag{11}$$

$$\begin{aligned} A(\alpha_1, \alpha_2, k) = \sum_{m=1}^{M} \sum_{n=1}^{2} \Big[& 3 \left| G_{1,\mathrm{RX}(m)}(k) G_{1,\mathrm{TX}(n)}(k) \right|^2 \\ & + (\alpha_1 + \alpha_2) \left| G_{2,\mathrm{RX}(m)}(k) G_{2,\mathrm{TX}(n)}(-k) \right|^2 \\ & + 3 \left| G_{1,\mathrm{RX}(m)}(k) G_{2,\mathrm{TX}(n)}(k) \right|^2 \\ & + (\alpha_1 + \alpha_2) \left| G_{2,\mathrm{RX}(m)}(k) G_{1,\mathrm{TX}(n)}(-k) \right|^2 \Big] \\ & + 2\mathrm{Re}\Big[\sum_{m_1=1}^{M} \sum_{m_2 \neq m_1}^{M} G_{1,\mathrm{RX}(m_1)}(k) G_{1,\mathrm{RX}(m_2)}(k) \\ & \times \left(G_{1,\mathrm{TX}(2)}(k) G_{1,\mathrm{TX}(1)}(k) + G^*_{2,\mathrm{TX}(1)}(k) G^*_{2,\mathrm{TX}(2)}(k) \right) \Big] \\ & + 2\mathrm{Re}\Big[\sum_{m_1=1}^{M-1} \sum_{m_2=m_1+1}^{M} \left(\left| G_{1,\mathrm{TX}(1)}(k) \right|^2 \right. \\ & + \left| G_{1,\mathrm{TX}(2)}(k) \right|^2 + \left| G_{2,\mathrm{TX}(1)}(k) \right|^2 \\ & \left. + \left| G_{2,\mathrm{TX}(2)}(k) \right|^2 \right) G_{1,\mathrm{RX}(m_1)}(k) G^*_{1,\mathrm{RX}(m_2)}(k) \Big] \\ & + (4M^2 + 2M) - (4M + 2) \sum_{m=1}^{M} \mathrm{Re}\Big[G_{1,\mathrm{RX}(m)}(k) \\ & \times G_{1,\mathrm{TX}(1)}(k) + G^*_{1,\mathrm{RX}(m)}(k) G^*_{1,\mathrm{TX}(2)}(k) \Big], \end{aligned} \tag{12}$$

$$\beta_M = \frac{E\left[\left| H^{(\mathrm{ii})}_{n,m}(k) / H^{(\mathrm{ii})}(k) \right|^2 \right]}{\left(E\left[\left| H^{(\mathrm{ii})}_{n,m}(k) \right|^2 \right] / E\left[\left| H^{(\mathrm{ii})}(k) \right|^2 \right] \right)}. \tag{13}$$

Here, $H^{(\mathrm{ii})}(k) = \sum_{m=1}^{M} (|H^{(\mathrm{ii})}_{1,m}(k)|^2 + |H^{(\mathrm{ii})}_{2,m}(k)|^2)$ and $H^{(\mathrm{ii})}_{n,m}(k)$ is the frequency response of the radio channel between transmitter n and receiver m with channel profile (ii) (infinite delay spread). Then, it is interesting to notice that the parameter β_M defined in (13) depends essentially on only the number of receivers M and that it is practically independent of the considered subcarrier k. For practically interesting numbers of receivers, the values of β_M are given in Table 1. Thus in summary, even though the SIR bound expressions in (10)–(13) appear somewhat complicated, they can anyway be evaluated directly without any data or system simulations, to assess the overall I/Q imbalance effects in the system at hand.

To give some first illustrations about the derived SIR expressions, we consider a 2×1 STC-OFDM system ($M = 1$) with 256 subcarriers. The quadrature mixer I/Q imbalance values as well as the branch difference filters for the two transmitters and one receiver are 4%, -4°, $[1, 0.04, -0.03]$ (TX1), 3%, 3°, $[1, -0.04, -0.03]$ (TX2), and 5%, 5°, $[1, 0.05]$ (RX). Here, in the branch difference filter models, the sample rate is assumed to be the 256th part of the corresponding OFDM symbol duration. Then, the resulting SIR due to

I/Q imbalances is evaluated using (10)–(13), assuming both frequency-flat (case (i)) and arbitrarily frequency-selective (case (ii)) radio channels. The results are shown in Figure 3, together with the corresponding simulated SIRs obtained using full system simulations with 64QAM as the subcarrier data modulation. In the system simulations, 25 000 independent channel and data symbol realizations are used to collect reliable sample statistics. Clearly, based on Figure 3, the system simulation results for the obtainable SIR fully match the derived analytical results, confirming the validity and correctness of the analysis. Figure 3 also demonstrates that even with reasonably mild frequency selectivity in the actual I/Q imbalances (as in this example), possibly combined with frequency-selective multipath radio channels (case (ii)), the achievable SIR is strongly frequency-selective varying from subcarrier to another. As an example, say, at subcarriers $k_1 = 40$ and $k_2 = -111$, these SIR ranges are 18.9–19.7 dB (k_1) and 20.8–22.8 dB (k_2), respectively, as can be read from Figure 3. To further illustrate this variation of the resulting signal quality as a function of subcarrier and also to get some visual justification for the reported SIR figures, the corresponding example detector input constellations (using 16QAM for readability) at the above example subcarriers $k_1 = 40$ and $k_2 = -111$ are shown in Figure 4 with channel type (i) (frequency-flat) and in Figure 5 with channel type (ii) (arbitrarily frequency-selective). Further examples and illustrations, together with actual detection error rate simulations, using extended vehicular A-type practical radio channels described in [26] will be given in Section 5.

4. PILOT-BASED I/Q IMBALANCE COMPENSATION

One possible way of approaching the I/Q imbalance compensation is to consider the I/Q matching of each individual front-end separately. This being the case, any of the earlier proposed compensation techniques targeted for single-antenna systems can basically be applied. Here, we take an alternative approach and try to mitigate the interference and distortion due to I/Q imbalances of each transmitter and receiver jointly on the receiver side, operating on the combiner output signal (7). As will be shown in what follows, this approach has one crucial practical benefit of being able to also compensate for the errors and signal distortion due to *channel estimation errors*, at zero extra cost. This is seen as being very important from any practical system point of view since channel estimation errors are anyway inevitable due to additive channel noise. In general, the compensator developments are here based on the rich algebraic structure of the derived signal model for the combiner output given in (7), combined with properly allocated pilot data. In general, the purpose of the compensation stage in our formulation is to estimate the data symbols $s_1(k)$ and $s_2(k)$ given the observed data $y_1(k)$ and $y_2(k)$.

4.1. Basic compensation idea and pilot allocation

All practical OFDM and/or MIMO-OFDM systems include some known pilot data for channel estimation purposes. Here, we also assume that such pilot signal is available. More specifically, we assume that four consecutive OFDM symbol periods (two STC blocks) are used for pilot purposes, during which the subcarrier data is allocated as[1]

$$\forall k : s_1^{(1)}(k) = s_P, \quad s_2^{(1)}(k) = s_P^*, \quad s_1^{(2)}(k) = s_P, \quad s_2^{(2)}(k) = s_P. \tag{14}$$

Here, s_P denotes the pilot data value (which can be considered as one of the design "parameters") and superscripts $^{(1)}$ and $^{(2)}$ refer to the two pilot blocks. With the above pilot allocation, the resulting subcarrier observations $y_1^{(1)}(k)$, $y_2^{(1)}(k)$, $y_1^{(2)}(k)$, $y_2^{(2)}(k)$ can be shown (see (7)) to yield a well-behaving 4×4 set of linear equations. Writing this in vector-matrix form yields

$$\mathbf{y}_P(k) = \mathbf{S}_P \boldsymbol{\theta}(k), \tag{15}$$

where $\mathbf{y}_P(k) = [y_1^{(1)}(k),\ y_2^{(1)}(k)^*,\ y_1^{(2)}(k),\ y_2^{(2)}(k)^*]^T$, $\boldsymbol{\theta}(k) = [a(k),\ b(k),\ c(k),\ d(k)]^T$, and

$$\mathbf{S}_P = \begin{bmatrix} s_P & s_P^* & s_P^* & s_P \\ s_P & s_P^* & -s_P^* & -s_P \\ s_P & s_P^* & s_P & s_P^* \\ s_P^* & s_P & -s_P^* & -s_P \end{bmatrix}. \tag{16}$$

Then, the coefficients $a(k)$, $b(k)$, $c(k)$, and $d(k)$ can be easily solved from (15) as

$$\hat{\boldsymbol{\theta}}(k) = \mathbf{S}_P^{-1} \mathbf{y}_P(k) \tag{17}$$

given that $\det(\mathbf{S}_P) = 2(s_P^2 - (s_P^*)^2)^2 \neq 0$ or $s_P^2 \neq (s_P^*)^2$. This, in turn, holds for any purely complex-valued training symbol s_P (i.e., both real and imaginary parts being nonzero). Notice also that the obvious symmetric structure of $\mathbf{S}_P$ in (16) yields great computational savings in solving (15) for $\boldsymbol{\theta}(k)$ in (17). More specifically, after some straightforward algebra, the inverse of $\mathbf{S}_P$ can be written as

$$\mathbf{S}_P^{-1} = \begin{bmatrix} A_1 & A_2 & 0 & A_4 \\ A_1 & -A_2 & 0 & A_3 \\ -A_2 & -A_1 & A_3 & 0 \\ A_2 & -A_1 & A_4 & 0 \end{bmatrix}, \tag{18}$$

where $A_1 = 1/(4\mathrm{Re}[s_P])$, $A_2 = 1/(4j\mathrm{Im}[s_P])$, $A_3 = s_P/(4j\mathrm{Re}[s_P]\mathrm{Im}[s_P])$, $A_4 = -s_P^*/(4j\mathrm{Re}[s_P]\mathrm{Im}[s_P])$.

Then, it is very interesting to notice that if the pilot symbol s_P is "designed" (selected) such that its real and imaginary parts are identical (e.g., $3+j3$), the inversion in (18) becomes almost trivial. Denoting such pilot symbol as $s_P = p + jp$, direct substitution and manipulations yield

$$\mathbf{S}_P^{-1} = \frac{1}{4p} \begin{bmatrix} 1 & -j & 0 & 1+j \\ 1 & j & 0 & 1-j \\ j & -1 & 1-j & 0 \\ -j & -1 & 1+j & 0 \end{bmatrix}. \tag{19}$$

[1] Conceptually, similar pilot design is used also in [16] in single-carrier STTD system context with time domain compensation processing.

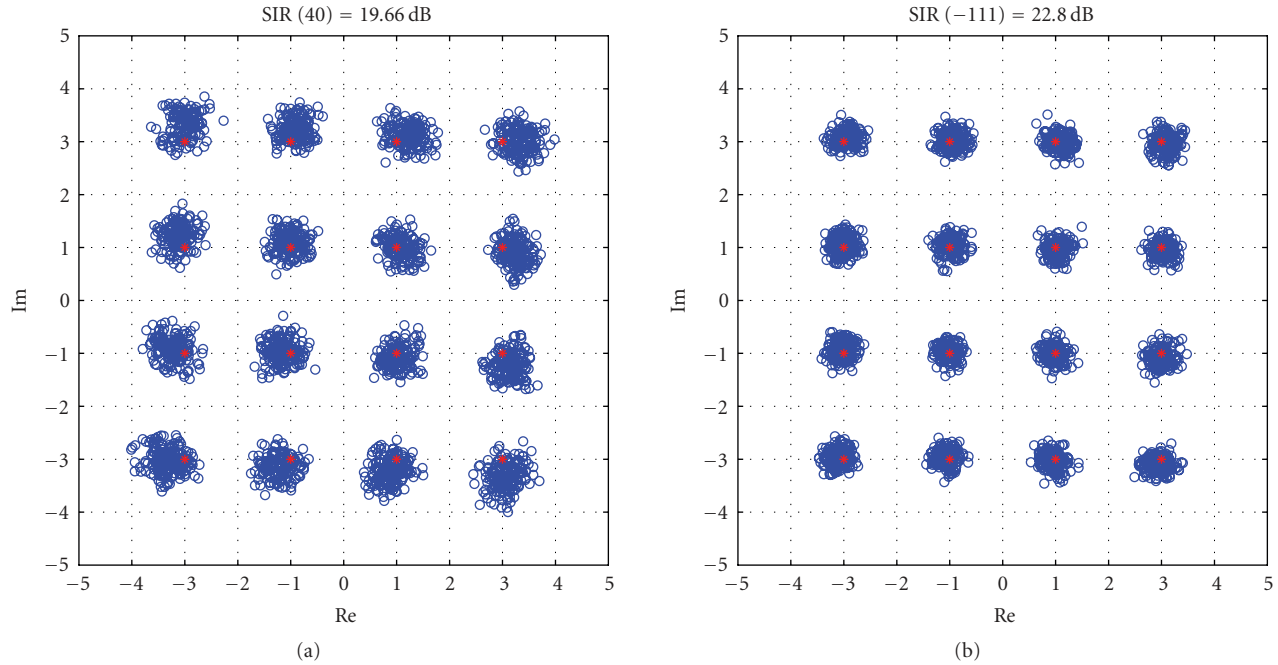

FIGURE 4: 16QAM detector input signal constellations at two example subcarriers numbers 40 and −111 in a 256-subcarrier 2 × 1 STC-OFDM system under frequency-selective TX and RX I/Q imbalances; independent realizations of frequency-flat radio channels (channel type (i)) and no additive noise.

So, the parameter estimation in (17) is close to trivial in terms of the needed computational complexity.

Now, having estimated the model coefficients for all the active subcarriers during the pilot slots, these estimates are then used during the actual data transmission for removing the interfering signal terms due to I/Q imbalance. During one STC data block, this can be done by collecting the observations $y_1(k)$, $y_2(k)$, $y_1(-k)$, and $y_2(-k)$ into $\mathbf{y}(k) = [y_1(k), y_1^*(-k), y_2(k), y_2^*(-k)]^T$, which, based on (6), yields

$$\mathbf{y}(k) = \hat{\mathbf{\Phi}}(k)\mathbf{s}(k), \tag{20}$$

where $\mathbf{s}(k) = [s_1(k), s_1^*(-k), s_2(k), s_2^*(-k)]^T$ and

$$\hat{\mathbf{\Phi}}(k) = \begin{bmatrix} \hat{a}(k) & \hat{b}(k) & \hat{c}(k) & \hat{d}(k) \\ \hat{b}^*(-k) & \hat{a}^*(-k) & \hat{d}^*(-k) & \hat{c}^*(-k) \\ -\hat{c}^*(k) & -\hat{d}^*(k) & \hat{a}^*(k) & \hat{b}^*(k) \\ -\hat{d}(-k) & -\hat{c}(-k) & \hat{b}(-k) & \hat{a}(-k) \end{bmatrix}. \tag{21}$$

In (20)-(21), the hat notation ($\hat{a}(k)$, etc.) refers to the estimated coefficients obtained during the pilot phase. Since the vector $\mathbf{s}(k)$ includes the data symbols (or their conjugates) at both mirror carriers k and $-k$, it is obvious that (20) needs to be solved only for each mirror-carrier pair. Assuming symmetric subcarrier deployment, which is the typical case, the overall compensator is given by

$$\hat{\mathbf{s}}(k) = \hat{\mathbf{\Phi}}(k)^{-1}\mathbf{y}(k), \quad k \in \Omega_+, \tag{22}$$

in which Ω_+ denotes the set of positive subcarrier indexes. Notice that again the inherent symmetric structure of the matrix $\hat{\mathbf{\Phi}}(k)$ in (21) yields great computational savings in practice, as opposed to full matrix inversion in (22).

4.2. Impact of I/Q imbalances on the channel estimation quality

The proposed compensation structure operates on the subcarrier data samples *after diversity combining*. This implies that some form of channel estimation is needed, as in any OFDM system, prior to the compensation stage. The previous derivations assumed ideal diversity combining with perfectly estimated channels, which is of course unrealistic. Both the additive noise and the I/Q imbalance result in erroneous channel estimates in practice. As a concrete practical example, the previous pilot allocation in (14) is assumed for channel estimation as well. Under pilot slot 1, with perfect I/Q balance and no additive noise, the outputs of the mth receiver FFT stage after CP removal are given by

$$\begin{aligned} x_{1,m}{}^{(p)}(k) &= H_{1,m}(k)s_P + H_{2,m}(k)s_P^*, \\ x_{2,m}{}^{(p)}(k) &= -H_{1,m}(k)s_P + H_{2,m}(k)s_P^*. \end{aligned} \tag{23}$$

This follows directly from (5) and (14). Then, the channel coefficients can be estimated as

$$\begin{pmatrix} \hat{H}_{1,m}(k) \\ \hat{H}_{2,m}(k) \end{pmatrix} = \begin{pmatrix} \dfrac{1}{(2s_P)} & \dfrac{-1}{(2s_P)} \\ \dfrac{1}{(2s_P^*)} & \dfrac{1}{(2s_P^*)} \end{pmatrix} \begin{pmatrix} x_{1,m}{}^{(p)}(k) \\ x_{2,m}{}^{(p)}(k) \end{pmatrix}, \tag{24}$$

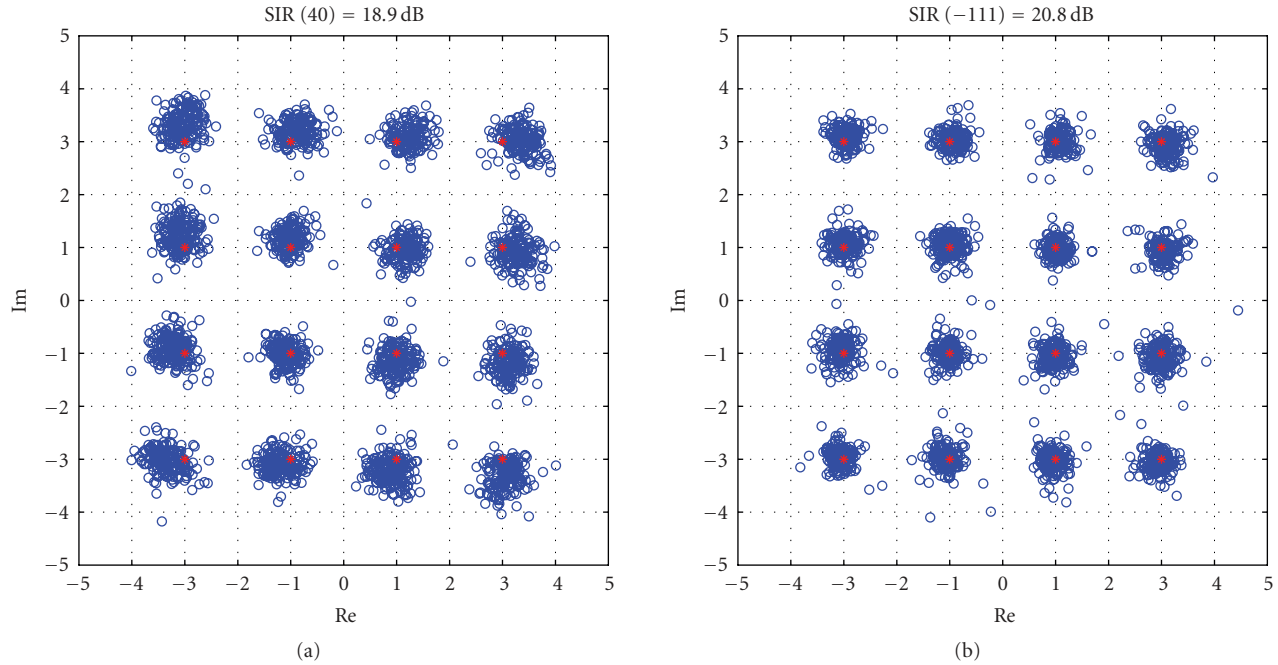

Figure 5: 16QAM detector input signal constellations at two example subcarriers numbers 40 and −111 in a 256-subcarrier 2 × 1 STC-OFDM system under frequency-selective TX and RX I/Q imbalances; independent realizations of arbitrarily frequency-selective radio channels (channel type (ii)) and no additive noise.

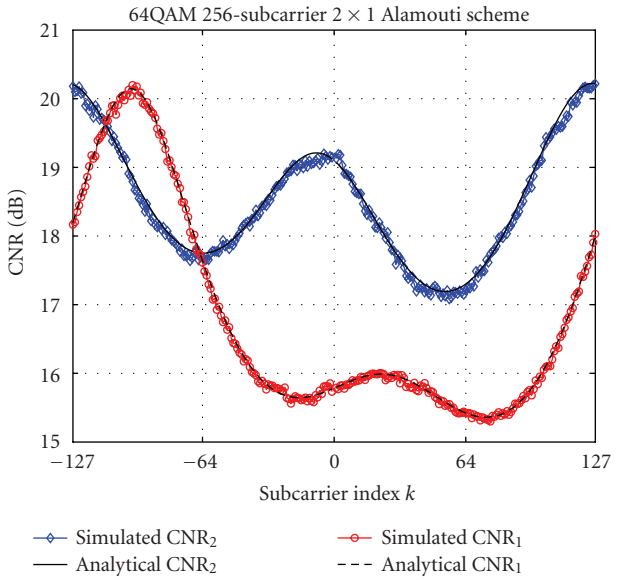

Figure 6: Channel estimation error figure of merits with transmitter and receiver I/Q imbalances and received SNR of 20 dB, as a function of subcarrier index k in a 2 × 1 256-subcarrier STC-OFDM system; extended vehicular A radio channels.

which follows directly from (23). Now, incorporating also the transmitter and receiver I/Q imbalances, together with additive noise, the resulting channel estimation errors $E_{1,m}(k) = \widehat{H}_{1,m}(k) - H_{1,m}(k)$ and $E_{2,m}(k) = \widehat{H}_{2,m}(k) - H_{2,m}(k)$ at the kth subcarrier in the mth receiver can be shown to be of the form

$$\begin{aligned}
E_{1,m}(k) &= H_{1,m}(k)\left[G_{1,\mathrm{RX}(m)}(k)G_{1,\mathrm{TX}(1)}(k) - 1\right] \\
&\quad + H^*_{1,m}(-k)G_{2,\mathrm{RX}(m)}(k)G^*_{2,\mathrm{TX}(1)}(-k) \\
&\quad + \left[H_{1,m}(k)G_{1,\mathrm{RX}(m)}(k)G_{2,\mathrm{TX}(1)}(k)\right. \\
&\quad \left. + H^*_{1,m}(-k)G_{2,\mathrm{RX}(m)}(k)G^*_{1,\mathrm{TX}(1)}(-k)\right]\left(\frac{s^*_P}{s_P}\right) \\
&\quad + \left[G_{1,\mathrm{RX}(m)}(k)\left(N_{1,m}(k) - N_{2,m}(k)\right)\right. \\
&\quad \left. + G_{2,\mathrm{RX}(m)}(k)\left(N^*_{1,m}(-k) - N^*_{2,m}(-k)\right)\right] \Big/ (2s_P), \\
E_{2,m}(k) &= H_{2,m}(k)\left[G_{1,\mathrm{RX}(m)}(k)G_{1,\mathrm{TX}(2)}(k) - 1\right] \\
&\quad + H^*_{2,m}(-k)G_{2,\mathrm{RX}(m)}(k)G^*_{2,\mathrm{TX}(2)}(-k) \\
&\quad + \left[H_{2,m}(k)G_{1,\mathrm{RX}(m)}(k)G_{2,\mathrm{TX}(2)}(k)\right. \\
&\quad \left. + H^*_{2,m}(-k)G_{2,\mathrm{RX}(m)}(k)G^*_{1,\mathrm{TX}(2)}(-k)\right]\left(\frac{s_P}{s^*_P}\right) \\
&\quad + \left[G_{1,\mathrm{RX}(m)}(k)\left(N_{1,m}(k) + N_{2,m}(k)\right)\right. \\
&\quad \left. + G_{2,\mathrm{RX}(m)}(k)\left(N^*_{1,m}(-k) + N^*_{2,m}(-k)\right)\right] \Big/ (2s^*_P),
\end{aligned} \tag{25}$$

where $N_{1,m}(k)$ and $N_{2,m}(k)$ are the noise samples at the FFT output (kth bin) of the mth receiver. Then, with realistic I/Q imbalance values and similar assumptions on the channel statistics described in Section 3, the impact of noise and I/Q imbalances on the quality of the channel estimation can

be assessed analytically. The so-called channel-to-noise ratio (CNR) at the kth subcarrier of the mth receiver, defined below, can now be shown to be of the form

$$\begin{aligned}
\mathrm{CNR}_{1,m}(k) &= \frac{E\left[\,|H_{1,m}(k)|^2\right]}{E\left[\,|E_{1,m}(k)|^2\right]} \\
&= 1\Big/\Big\{\Big|G_{1,\mathrm{RX}(m)}(k)\Big(G_{1,\mathrm{TX}(1)}(k)+\Big(\frac{s_P^*}{s_P}\Big)G_{2,\mathrm{TX}(1)}(k)\Big) \\
&\quad -1\Big|^2+\Big|G_{2,\mathrm{RX}(m)}(k)\Big(G^*_{2,\mathrm{TX}(1)}(-k) \\
&\quad +\Big(\frac{s_P^*}{s_P}\Big)G^*_{1,\mathrm{TX}(1)}(-k)\Big)\Big|^2+(|G_{1,\mathrm{RX}(m)}(k)|^2 \\
&\quad +|G_{2,\mathrm{RX}(m)}(k)|^2)/(\gamma_m\times\sigma_p)\Big\}, \\
\mathrm{CNR}_{2,m}(k) &= \frac{E\left[\,|H_{2,m}(k)|^2\right]}{E\left[\,|E_{2,m}(k)|^2\right]} \\
&= 1\Big/\Big\{\Big|G_{1,\mathrm{RX}(m)}(k)\Big(G_{1,\mathrm{TX}(2)}(k)+\Big(\frac{s_P}{s_P^*}\Big)G_{2,\mathrm{TX}(2)}(k)\Big) \\
&\quad -1\Big|^2+\Big|G_{2,\mathrm{RX}(m)}(k)\Big(G^*_{2,\mathrm{TX}(2)}(-k) \\
&\quad +\Big(\frac{s_P}{s_P^*}\Big)G^*_{1,\mathrm{TX}(2)}(-k)\Big)\Big|^2+(|G_{1,\mathrm{RX}(m)}(k)|^2 \\
&\quad +|G_{2,\mathrm{RX}(m)}(k)|^2)/(\gamma_m\times\sigma_p)\Big\},
\end{aligned} \tag{26}$$

respectively, where γ_m is the average receiver input signal-to-noise ratio at receiver m and σ_p is ratio of the used pilot data power to the average power of the data constellation. The expressions in (26) clearly indicate that, in addition to traditional additive noise effect, the I/Q imbalances in transmitter and receiver radio front-ends are also having a clear impact on the *channel estimation quality*. In effect, with zero additive noise, the CNRs in (26) are upper-bounded due to I/Q imbalances alone by

$$\begin{aligned}
\mathrm{CNR}^{\max}_{1,m}(k) &= 1\Big/\Big(\Big|G_{1,\mathrm{RX}(m)}(k)\Big(G_{1,\mathrm{TX}(1)}(k)+\frac{s_P^*}{s_P}G_{2,\mathrm{TX}(1)}(k)\Big) \\
&\quad -1\Big|^2+\Big|G_{2,\mathrm{RX}(m)}(k)\Big(G^*_{2,\mathrm{TX}(1)}(-k) \\
&\quad +\frac{s_P^*}{s_P}G^*_{1,\mathrm{TX}(1)}(-k)\Big)\Big|^2\Big), \\
\mathrm{CNR}^{\max}_{2,m}(k) &= 1\Big/\Big(\Big|G_{1,\mathrm{RX}(m)}(k)\Big(G_{1,\mathrm{TX}(2)}(k)+\frac{s_P}{s_P^*}G_{2,\mathrm{TX}(2)}(k)\Big) \\
&\quad -1\Big|^2+\Big|G_{2,\mathrm{RX}(m)}(k)\Big(G^*_{2,\mathrm{TX}(2)}(-k) \\
&\quad +\frac{s_P}{s_P^*}G^*_{1,\mathrm{TX}(2)}(-k)\Big)\Big|^2\Big).
\end{aligned} \tag{27}$$

Using a similar numerical example as earlier (2×1 STC-OFDM system, 256 subcarriers, and 64QAM subcarrier data modulation), with the imbalance parameters of the two transmitters and one receiver being 4%, -4°, $[1, 0.04, -0.03]$ (TX1), 3%, 3°, $[1, -0.04, -0.03]$ (TX2), and 5%, 5°, $[1, 0.05]$ (RX), respectively, the resulting CNRs are here evaluated using both the analytical expression in (26) as well as the actual data/system simulations. In the system simulations, the used radio channels are random realizations of the extended vehicular A model [26], and channel estimation is implemented as given in (24). The used pilot data value s_P is the right upper corner symbol ($7 + j7$) of the used 64QAM constellation, corresponding to $\sigma_p = 2.33$ (or roughly 3.5 dB pilot "boost" compared to average symbol power). The obtained results for the channel estimation quality are presented in Figures 6 and 7. Figure 6 shows both the simulated and the analytical CNRs for different subcarriers at a fixed received SNR of 20 dB, while Figure 7 presents the CNR behavior at example subcarrier no. 40 as a function of additive noise SNR. Altogether, these demonstrate clearly that the CNR figures obtained using system simulations match the analytical analysis very accurately. In Figure 7, the curves also clearly saturate to the derived upper bounds in (27) due to I/Q imbalance alone, which in this case are 16.7 dB and 18.7 dB as can easily be evaluated using (27). It is also very interesting to notice that in this example, the channel estimation qualities are relatively different for the two channels (TX(1)-to-RX and TX(2)-to-RX) due to different I/Q imbalances, even if the additive noise SNRs are identical at the receiver input. Thus, in general, the above CNR analysis shows that I/Q imbalances can easily become a limiting factor *also from the channel estimation point of view* in future multiantenna wireless OFDM systems. Thus, devising techniques that can compensate for channel estimation inaccuracies are seen generally as an important and interesting task.

4.3. Impact of channel estimation errors on the combiner output signal

Next, we consider the effect of using imperfect channel knowledge or channel estimates $\widehat{H}_{1,m}(k)$ and $\widehat{H}_{2,m}(k)$, $m = 1, 2, \ldots, M$, in the diversity combining stage, including also the I/Q imbalance effects of the individual transmitters and receivers as discussed earlier. Now, it is relatively straightforward to show that for arbitrary channel estimates $\widehat{H}_{1,m}(k)$ and $\widehat{H}_{2,m}(k)$, the combiner output samples are given by

$$\begin{aligned}
y'_1(k) &= a'(k)s_1(k)+b'(k)s_1^*(-k)+c'(k)s_2(k)+d'(k)s_2^*(-k), \\
y'_2(k) &= a'^*(k)s_2(k)+b'^*(k)s_2^*(-k) \\
&\quad -c'^*(k)s_1(k)-d'^*(k)s_1^*(-k),
\end{aligned} \tag{28}$$

in which the exact expressions for the modified system coefficients ($a'(k)$, $b'(k)$, $c'(k)$, and $d'(k)$) are given in (29). Thus in general, it is very interesting to notice that the derived

system model above is structurally identical to the one derived earlier (assuming perfect channel knowledge) in (7)-(8). The only difference lies in the more detailed and complicated structure of the system coefficients ($a'(k)$, $b'(k)$, $c'(k)$, and $d'(k)$). This, in turn, shows that the mirror subcarrier-wise estimation-compensation processing described in (15)–(22) can, by design, simultaneously mitigate the effects of both I/Q imbalance and channel estimation inaccuracies. This is a very important practical benefit and will be illustrated and demonstrated in more detail in what follows using computer simulations:

$$
\begin{aligned}
a'(k) = \sum_{m=1}^{M} & (\widehat{H}^{*}_{1,m}(k)H_{1,m}(k)G_{1,\mathrm{RX}(m)}(k)G_{1,\mathrm{TX}(1)}(k) \\
& + \widehat{H}^{*}_{1,m}(k)H^{*}_{1,m}(-k)G_{2,\mathrm{RX}(m)}(k)G^{*}_{2,\mathrm{TX}(1)}(-k) \\
& + \widehat{H}_{2,m}(k)H^{*}_{2,m}(k)G^{*}_{1,\mathrm{RX}(m)}(k)G^{*}_{1,\mathrm{TX}(2)}(k) \\
& + \widehat{H}_{2,m}(k)H_{2,m}(-k)G^{*}_{2,\mathrm{RX}(m)}(k)G_{2,\mathrm{TX}(2)}(-k)), \\
b'(k) = \sum_{m=1}^{M} & (\widehat{H}^{*}_{1,m}(k)H_{1,m}(k)G_{1,\mathrm{RX}(m)}(k)G_{2,\mathrm{TX}(1)}(k) \\
& + \widehat{H}^{*}_{1,m}(k)H^{*}_{1,m}(-k)G_{2,\mathrm{RX}(m)}(k)G^{*}_{1,\mathrm{TX}(1)}(-k) \\
& + \widehat{H}_{2,m}(k)H^{*}_{2,m}(k)G^{*}_{1,\mathrm{RX}(m)}(k)G^{*}_{2,\mathrm{TX}(2)}(k) \\
& + \widehat{H}_{2,m}(k)H_{2,m}(-k)G^{*}_{2,\mathrm{RX}(m)}(k)G_{1,\mathrm{TX}(2)}(-k)), \\
c'(k) = \sum_{m=1}^{M} & (\widehat{H}^{*}_{1,m}(k)H_{2,m}(k)G_{1,\mathrm{RX}(m)}(k)G_{1,\mathrm{TX}(2)}(k) \\
& + \widehat{H}^{*}_{1,m}(k)H^{*}_{2,m}(-k)G_{2,\mathrm{RX}(m)}(k)G^{*}_{2,\mathrm{TX}(2)}(-k) \\
& - H^{*}_{1,m}(k)\widehat{H}_{2,m}(k)G^{*}_{1,\mathrm{RX}(m)}(k)G^{*}_{1,\mathrm{TX}(1)}(k) \\
& - H_{1,m}(-k)\widehat{H}_{2,m}(k)G^{*}_{2,\mathrm{RX}(m)}(k)G_{2,\mathrm{TX}(1)}(-k)), \\
d'(k) = \sum_{m=1}^{M} & (\widehat{H}^{*}_{1,m}(k)H_{2,m}(k)G_{1,\mathrm{RX}(m)}(k)G_{2,\mathrm{TX}(2)}(k) \\
& + \widehat{H}^{*}_{1,m}(k)H^{*}_{2,m}(-k)G_{2,\mathrm{RX}(m)}(k)G^{*}_{1,\mathrm{TX}(2)}(-k) \\
& - H^{*}_{1,m}(k)\widehat{H}_{2,m}(k)G^{*}_{1,\mathrm{RX}(m)}(k)G^{*}_{2,\mathrm{TX}(1)}(k) \\
& - H_{1,m}(-k)\widehat{H}_{2,m}(k)G^{*}_{2,\mathrm{RX}(m)}(k)G_{1,\mathrm{TX}(1)}(-k)).
\end{aligned}
\tag{29}
$$

Using the above signal models in (28)-(29), the earlier SIR analysis in Section 3 can also be extended to analyze the corresponding system-level SIR under the pilot-based channel estimation of (24) (as opposed to perfect channel knowledge assumed in Section 3). The results are given in the appendix. Notice, however, that the earlier derivations in (9)–(13) are of more general nature, in the sense of describing the system-level performance degradation due to I/Q imbalances alone in otherwise ideal system, while the extended analysis in the appendix is explicitly bound to the proposed channel estimation scheme. Under the pilot-based channel estimation scheme of (24), the extended analysis can be used to predict the detection error rates floors (due to I/Q imbalances and channel estimation errors) at high SNR.

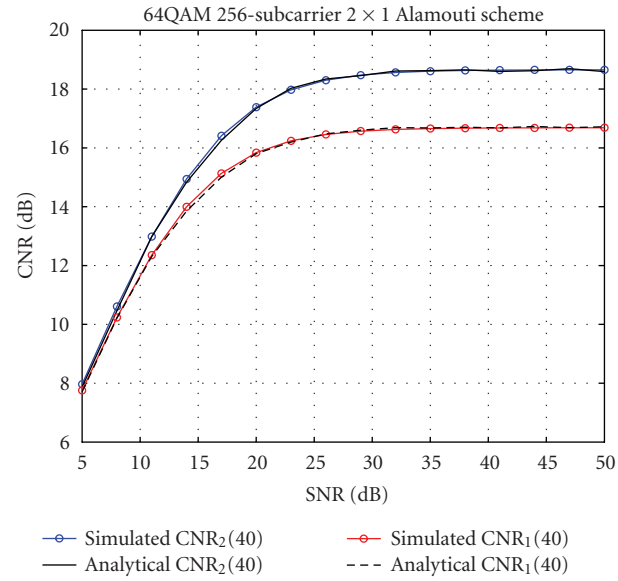

Figure 7: Channel estimation error figure of merits at subcarrier number 40 with transmitter and receiver I/Q imbalances, as a function of received SNR in a 2 × 1 256-subcarrier STC-OFDM system; extended vehicular A radio channels.

4.4. Other practical aspects

One essential element in the design and implementation of any multicarrier system is the frequency synchronization. Here, since the estimator/compensator is operating after the receiver FFTs, it is clear that relatively accurate carrier synchronization is needed, prior to FFT. This can be seen as one practical limitation. It should be noticed, however, that accurate carrier synchronization is needed in the considered STC-OFDM system context anyway, even with perfect I/Q balance. So in this sense, the requirements for carrier synchronization are coming mainly from the transmission technique itself, not from the compensation principle as such.

5. NUMERICAL ILLUSTRATIONS AND PERFORMANCE SIMULATIONS

5.1. SIR analysis and system-level performance in the presence of I/Q imbalance

In this section, the validity and meaning of the SIR analysis results in practical mobile radio channels are illustrated using computer simulations. 64QAM is used as the subcarrier data modulation and the number of OFDM subcarriers is $N = 256$, with subcarrier spacing of 120 kHz. The power-delay profiles of the individual radio channels between the transmitters and the receiver(s) follow the extended vehicular A profile described in [26], having roughly 2.5-microsecond delay spread. As usual, proper cyclic prefix (CP) is always

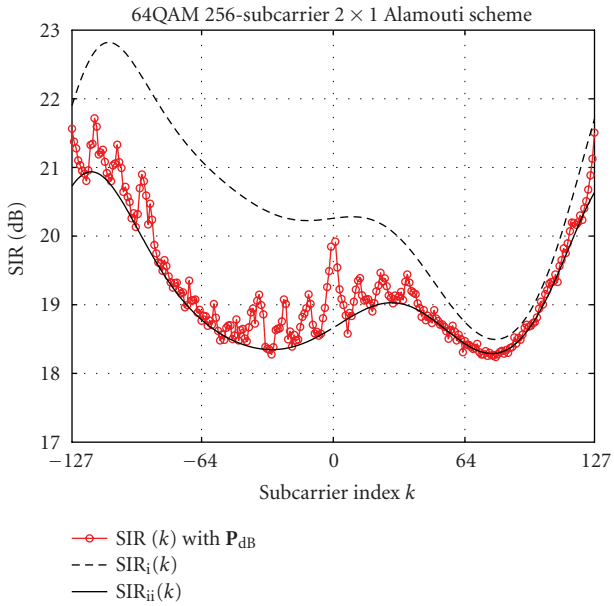

Figure 8: Example 1: SIR as a function of the subcarrier index k in a 2×1 STC-OFDM system with realistic frequency-selective I/Q imbalances at both transmitter and receiver analog front-ends; extended vehicular A radio channels ($\mathbf{P}_{\text{dB}}$). The dashed and solid lines show the analytical SIR values corresponding to the frequency-flat and arbitrarily frequency-selective fading cases, respectively.

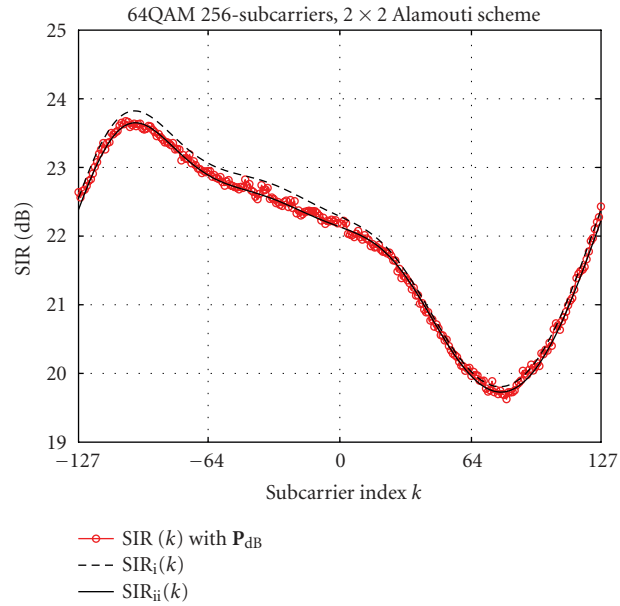

Figure 9: Example 2: SIR as a function of the subcarrier index k in a 2×2 STC-OFDM system with realistic frequency-selective I/Q imbalances at both transmitter and receiver analog front-ends; extended vehicular A radio channels ($\mathbf{P}_{\text{dB}}$). The dashed and solid lines show the analytical SIR values corresponding to the frequency-flat and arbitrarily frequency-selective fading cases, respectively.

used on the transmitter side and discarded in the receiver prior to the FFT. The individual channel tap realizations are chosen independently from complex Gaussian distribution and are assumed to be constants over two consecutive OFDM symbol periods [5], after which new channel realizations are drawn.

First, say, example 1, the 2×1 STC-OFDM case with earlier I/Q imbalance parameters of 4%, $-4°$, $[1, 0.04, -0.03]$ (TX1), 3%, $3°$, $[1, -0.04, -0.03]$ (TX2), and 5%, $5°$, $[1, 0.05]$ (RX) is examined. Using (4), the individual TX and RX front-end image attenuations are then ranging between 23.3 dB and 49.8 dB (TX1), 25 dB and 43.5 dB (TX2), and 22.5 dB and 32 dB (RX), varying rather smoothly as a function of frequency from subcarrier to another. The resulting average subcarrierwise SIRs, evaluated numerically with 25 000 independent channel and data symbol realizations, are then shown in Figure 8. The figure also shows the upper and lower bounds for the SIRs at each subcarrier, based on the analytical analysis presented in Section 3, corresponding to the frequency-flat and arbitrarily frequency-selective fading channels. Clearly, the analytical calculations are predicting the actual SIR behavior with realistic radio channels very accurately. This is further demonstrated by another similar example, example 2, considering the corresponding 2×2 STC-OFDM case. Thus, compared to example 1, one more receiver is added, with example imbalance parameters of 4%, $-5°$, $[1, -0.03, 0.04]$. Then, similarly as above, the actual subcarrierwise SIRs are evaluated numerically using simulations, shown in Figure 9, together with the corresponding analytical bounds. Again, it is obvious that the analytical analysis describes the essential SIR behavior very accurately.

In general, it is interesting to notice that the overall SIR levels are *considerably lower* than what might have been expected considering the qualities (IRRs) of the individual radios alone. This is indeed due to the interaction of the individual radio impairments and the space-time coding principle in the considered multiantenna scenario, and it is nicely incorporated in the system-level SIR analysis philosophy presented in Section 3. Thus, in multiantenna systems with multiple parallel radios, such system-level performance analysis and measures can be seen as being more appropriate and valid than the traditional IRR measures alone, focusing on individual radios. Furthermore, based on the obtained results and shown illustrations, it can be concluded that the RF impairments like I/Q mismatch will in general play a critical role in the future multiantenna wireless system evolutions.

Next, we assess the actual detection error performance of the overall system by comprehensive system simulations. Even though the interference due to I/Q imbalance is not exactly Gaussian, the derived SIR values do indeed predict the high-SNR behavior of the detection error rates very accurately, as the following simulations show. Here, the earlier 2×1 STC-OFDM case with 256 subcarriers is assumed and the symbol error rates (SERs) at example subcarriers numbers 40 and -111 are evaluated by system simulations. 25 000 64QAM symbols are transmitted, per subcarrier, and the radio channels are again following the extended vehicular A power-delay profile. The obtained SER results are depicted

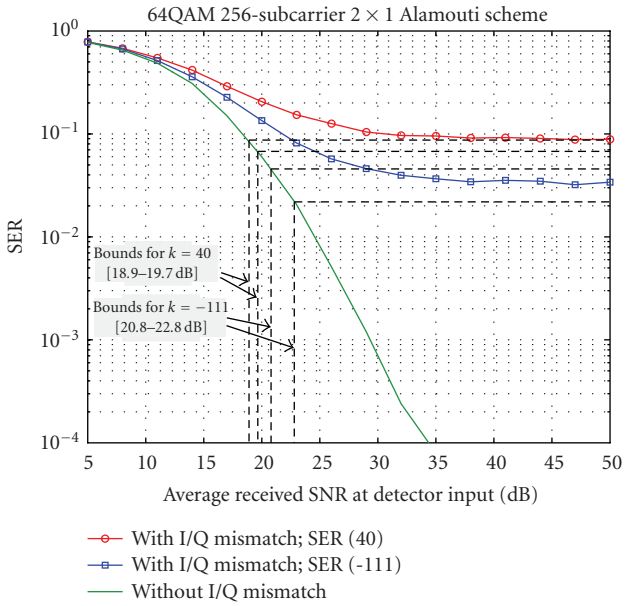

FIGURE 10: Simulated 64QAM symbol error rates at example subcarriers numbers 40 and −111; 2 × 1 STC-OFDM system with 256 subcarriers and realistic frequency-selective I/Q imbalances at both TX and RX analog front-ends; extended vehicular A radio channels. The figure also shows the high-SNR error floors using the SIR analysis results.

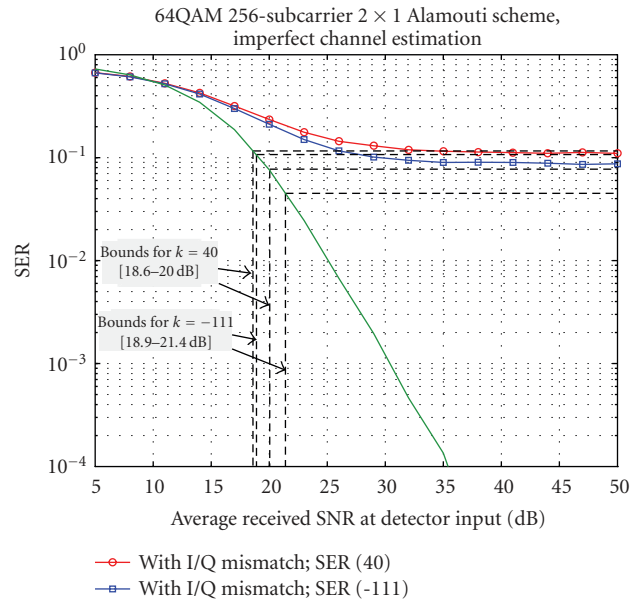

FIGURE 11: Simulated 64QAM symbol error rates at example subcarriers numbers 40 and −111; 2 × 1 STC-OFDM system with 256 subcarriers and realistic frequency-selective I/Q imbalances at both TX and RX analog front-ends; extended vehicular A radio channels and pilot-based channel estimation in the diversity combining stage. The figure also shows the high-SNR error floors using the extended SIR analysis results of the appendix.

in Figure 10 as a function of the average signal-to-noise ratio (SNR) due to channel noise at the detector input. The figure also shows the SER values corresponding to the derived SIR ranges of 18.9–19.66 dB (subcarrier no. 40) and 20.8–22.8 dB (subcarrier no. −111), evaluated at the corresponding SNRs for the perfectly balanced system. Obviously, the analysis predicts very accurately the high-SNR behavior and the resulting SER floor due to I/Q imbalance. This further demonstrates the validity of the analysis as a valuable analytical system-level tool in the system design and dimensioning. Similar illustration is given in Figure 11 in which also the effects of using the pilot-based channel estimates in the diversity combining stage are taken into account. The corresponding analytical analysis for the SIR bounds under channel estimation is given in the appendix. Clearly, the analysis is again able to predict the high-SNR error floors accurately. It is also obvious that the error rates are increased (due to imperfect channel knowledge) compared to Figure 10.

5.2. *The efficiency of pilot-based I/Q imbalance compensation*

Next, the overall system performance with the proposed imbalance compensation scheme included is evaluated in terms of the detection error rates. The same system of 2 × 1 STC-OFDM with 256 subcarriers as discussed earlier is again assumed, together with the similar transmitter and receiver I/Q imbalances. The used subcarrier data modulation is 64QAM, and again the radio channels are random realizations of the extended vehicular A model. Here, to keep the pilot overhead reasonable, a quasistatic system model is assumed such that the channel coefficients are assumed to be fixed over 100 consecutive OFDM symbol intervals, after which new channel realizations are drawn. Different amounts of pilot symbols are tested and the pilots always appear in the beginning of the 100 symbol frames and they are used for channel estimation as well as imbalance parameter estimation, as described in Section 4. The upper right corner symbol " $7 + j7$ " of the used 64QAM constellation is used as the pilot data s_P. This corresponds to roughly 3.5 dB "pilot boosting" compared to average constellation power, which is a rather typical value in any OFDM system. Altogether, 100 000 symbols per subcarrier are transmitted and used in evaluating the symbol error rates (SERs), and the number of different channel realizations is 1000.

Figure 12 shows the system SER performance with different numbers of pilot slots, averaged over all subcarriers. Here, one slot refers to a pair of pilot blocks allocated as given in (14). With multiple slots, averaging is used over the individual parameter estimates to decrease the additive noise effects. Also shown are the uncompensated and perfectly matched reference system cases as well. Clearly, with just a few pilot slots, SER performance being practically identical to the reference system can be obtained using the proposed approach. Figure 13, in turn, shows the corresponding SER performance when also the channel frequency responses ($H_{1,1}(k)$ and $H_{2,1}(k)$ here) are estimated using (24), together

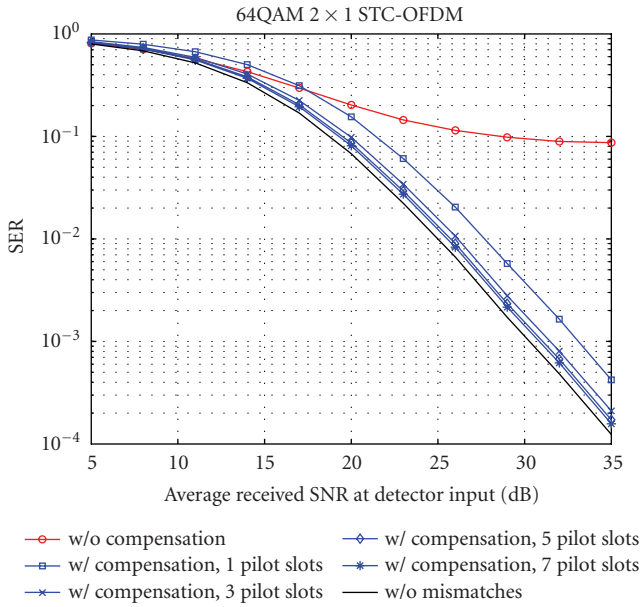

Figure 12: Simulated 64QAM symbol error rates, averaged for all subcarriers, with and without the proposed compensation technique, with different amounts of pilot symbols used for imbalance parameter estimation in the receiver; 2 × 1 STC-OFDM system case and realistic frequency-selective I/Q imbalances at both TX and RX analog front-ends; extended vehicular A radio channels; and channel estimation is assumed to be perfect.

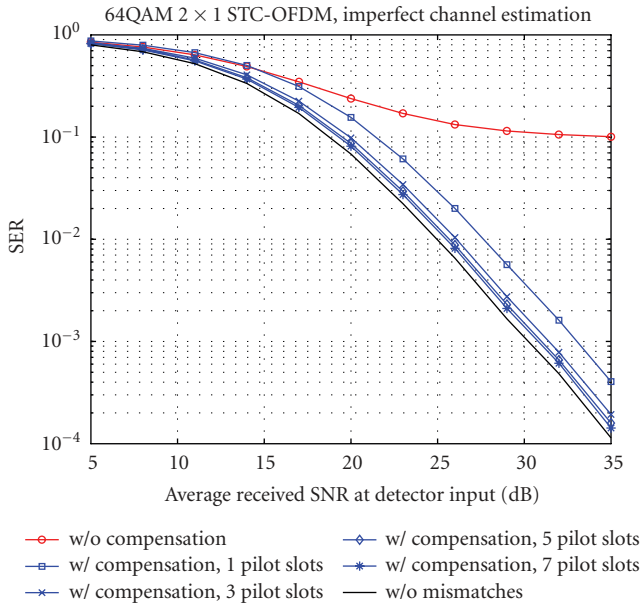

Figure 13: Simulated 64QAM symbol error rates, averaged for all subcarriers, with and without the proposed compensation technique, with different amounts of pilot symbols used for imbalance parameter as well as channel response estimations in the receiver; 2 × 1 STC-OFDM system case and realistic frequency-selective I/Q imbalances at both TX and RX analog front-ends; extended vehicular A radio channels.

with the model coefficients, using the given pilot allocation in (14). Due to noise and I/Q imbalance, this obviously results in errors in the estimated channel coefficients used in the combining stage. However, as shown by Figure 13, the overall system performance remains practically unchanged in the compensated case. This shows robustness against channel estimation errors in general, which was established also analytically in Section 4, stemming from the structural similarity of the overall system models with and without channel estimation errors. This is generally seen as a very important practical asset, related to the proposed estimation-compensation scheme, which cannot be established to any other reference solution in the literature.

6. CONCLUSIONS

This paper addressed the radio implementation-related RF impairment, called I/Q imbalance, in the space-time coded multiantenna OFDM system context. The challenging yet practical case of having frequency-dependent I/Q imbalances in all the individual radio transmitters and receivers was considered, which is essential in the future system developments with bandwidths in the order of several or tens of MHz. The overall signal distortion due to the I/Q imbalances was first analyzed analytically, in terms of signal-to-interference ratio (SIR), taking into account also the individual fading multipath channels between the transmitters and receivers. Two extreme cases were considered in detail, with either frequency-flat or independent subcarrier fading characteristics, within which all the practical fading and multipath profiles then fitted. The derived SIR values are subcarrier-specific and give an upper bound on the achievable overall signal-to-interference-and-noise ratio (SINR) in the system prior to data detection. Thus, the SIR analysis results can be used to assess the impact of I/Q imbalances on the system performance without lengthy data and system simulations, and therefore they give a valuable tool for the system and transceiver designers. Furthermore, the impact of I/Q imbalances and noise on the channel estimation stage was also evaluated and quantified in terms of channel-to-noise ratio (CNR) analysis. Stemming from the derived signal models, a pilot-based estimator-compensator structure was then proposed for jointly mitigating the I/Q imbalance effects due to imperfections of the individual radio front-ends. The compensation is carried out in a subcarrierwise manner at the output of the receiver diversity combining stage. The compensation structure was further shown, both by computer simulations as well as analytical signal modeling, to compensate for the channel estimation errors as well, with zero extra cost. In general, comprehensive system simulations were used to demonstrate that all the essential signal distortion due to I/Q imbalances and channel estimation errors can be cancelled with low pilot overhead, using the proposed compensator. The future work includes building a real-time FPGA demonstrator and a prototype for the overall receiver signal processing stages, including channel estimation, diversity combining, and impairment estimator-compensator blocks.

APPENDIX

A. EXTENDED SIR ANALYSIS INCLUDING CHANNEL ESTIMATION

Here, the SIR at the output of the receiver diversity combiner is derived including the effects of imperfect channel knowledge. From the channel noise point of view, high-SNR assumption is made, which corresponds to assessing the system behavior and the resulting detection error rate floors due to the interference alone. Now, assuming that the pilot-based channel estimator in (24) is used, the combiner output signals are generally given by (28)-(29). Then, similar to (9), the SIR is defined as

$$\begin{aligned}\mathrm{SIR}'(k) &= \frac{E\left[\,|s_1(k)|^2\right]}{E\left[\left|\dfrac{y'_1(k)}{\hat{H}(k)} - s_1(k)\right|^2\right]} \\ &\approx 1\Big/\left(E\left[\left|\frac{a'(k)}{H(k)} - 1\right|^2\right] + E\left[\left|\frac{b'(k)}{H(k)}\right|^2\right]\right. \\ &\quad \left. + E\left[\left|\frac{c'(k)}{H(k)}\right|^2\right] + E\left[\left|\frac{d'(k)}{H(k)}\right|^2\right]\right),\end{aligned} \tag{A.1}$$

where the system coefficients $a'(k)$, $b'(k)$, $c'(k)$, and $d'(k)$ are given in (29) and include the effects of both TX and RX I/Q imbalances as well as the imperfect channel knowledge. In (A.1), to make the analysis feasible, a simplifying approximation of $\hat{H}(k) \approx H(k)$ is made for the amplitude normalization term in which $H(k) = \sum_{m=1}^{M}(|H_{1,m}(k)|^2 + |H_{2,m}(k)|^2)$ and $\hat{H}(k) = \sum_{m=1}^{M}(|\hat{H}_{1,m}(k)|^2 + |\hat{H}_{2,m}(k)|^2)$. This is partially because the channel estimation errors $E_{1,m}(k) = \widehat{H}_{1,m}(k) - H_{1,m}(k)$ and $E_{2,m}(k) = \widehat{H}_{2,m}(k) - H_{2,m}(k)$ given in (25) are correlated with the true channel responses $H_{1,m}(k)$ and $H_{2,m}(k)$, as it is easily seen (see (25)). Then, using similar analysis principles and assumptions as in Section 3, the above SIR can be bound, depending on the type of the radio channels (frequency-flat and arbitrarily frequency-selective cases, see Section 3), as $\mathrm{SIR}'_{(\mathrm{ii})}(k) \le \mathrm{SIR}'(k) \le \mathrm{SIR}'_{(\mathrm{i})}(k)$, where now

$$\begin{aligned}\mathrm{SIR}'_{(\mathrm{i})}(k) &\approx \mathrm{SIR}'_{\mathrm{def}}(2, 1, k), \\ \mathrm{SIR}'_{(\mathrm{ii})}(k) &\approx \mathrm{SIR}'_{\mathrm{def}}(\beta_M, \beta_M, k), \\ \mathrm{SIR}'_{\mathrm{def}}(\alpha_1, \alpha_2, k) &= \frac{(2M + 4M^2)}{A'(\alpha_1, \alpha_2, k)}.\end{aligned} \tag{A.2}$$

The exact expression for $A'(\alpha_1, \alpha_2, k)$ is given in (A.3) and β_M is defined earlier in (13). Compared to (12), the expression in (A.3) is highly complicated due to the imperfect channel knowledge. Altogether, (A.2)-(A.3) give a system-level performance measure for $2 \times M$ STC-OFDM systems under frequency-selective TX and RX I/Q imbalances assuming the given pilot-based channel estimation in (24). Similar to (10)–(13), (A.2)-(A.3) can be used, for example, to analytically predict the high-SNR detection error rates in the system. This is illustrated in Section 5:

$$\begin{aligned}&A'(a_1, a_2, k) \\ &= \sum_{m=1}^{M}\sum_{n_1}^{2}\sum_{n_2\neq n_1}^{2} \\ &\quad \times\Bigg[\left(2\left|G^*_{1,\mathrm{TX}(n_1)}(k) + \frac{G^*_{2,\mathrm{TX}(n_1)}(k)s_p^*}{s_p}\right|^2\right. \\ &\qquad \left. + \left|G^*_{1,\mathrm{TX}(n_2)}(k) + \frac{G^*_{2,\mathrm{TX}(n_2)}(k)s_p^*}{s_p}\right|^2\right)|G_{1,\mathrm{RX}(m)}(k)|^4 \\ &\qquad \times\left(|G_{1,\mathrm{TX}(n_1)}(k)|^2 + |G_{2,\mathrm{TX}(n_1)}(k)|^2\right) \\ &\qquad + \left(\alpha_1\left|\left(G_{2,\mathrm{TX}(n_1)}(-k) + \frac{G_{1,\mathrm{TX}(n_1)}(-k)s_p^*}{s_p}\right)\right|^2\right. \\ &\qquad \left. + \alpha_2\left|G_{2,\mathrm{TX}(n_2)}(-k) + \frac{G_{1,\mathrm{TX}(n_2)}(-k)s_p^*}{s_p}\right|^2\right) \\ &\qquad \times|G_{1,\mathrm{RX}(m)}(k)G^*_{2,\mathrm{RX}(m)}(k)|^2\left(|G_{1,\mathrm{TX}(n_1)}(k)|^2 + |G_{2,\mathrm{TX}(n_1)}(k)|^2\right) \\ &\qquad + \left(\alpha_1\left|G^*_{1,\mathrm{TX}(n_1)}(k) + \frac{G^*_{2,\mathrm{TX}(n_1)}(k)s_p^*}{s_p}\right|^2\right. \\ &\qquad \left. + \alpha_2\left|G^*_{1,\mathrm{TX}(n_2)}(k) + \frac{G^*_{2,\mathrm{TX}(n_2)}(k)s_p^*}{s_p}\right|^2\right) \\ &\qquad \times|G_{2,\mathrm{RX}(m)}(k)G^*_{1,\mathrm{RX}(m)}(k)|^2 \\ &\qquad \times\left(|G_{1,\mathrm{TX}(n_1)}(-k)|^2 + |G_{2,\mathrm{TX}(n_1)}(-k)|^2\right)\Bigg] \\ &\quad +2\mathrm{Re}\Bigg[\sum_{m_1=1}^{M}\sum_{m_2\neq m_1}^{M}\left(|G_{1,\mathrm{RX}(m_1)}(k)|^2|G_{1,\mathrm{RX}(m_2)}(k)|^2\right) \\ &\qquad \times\prod_{n=1}^{2}\left(G^*_{1,\mathrm{TX}(n)}(k) + \frac{G^*_{2,\mathrm{TX}(n)}(k)s_p^*}{s_p}\right) \\ &\qquad \times\left(G_{1,\mathrm{TX}(1)}(k)G_{1,\mathrm{TX}(2)}(k) + G_{2,\mathrm{TX}(1)}(k)G_{2,\mathrm{TX}(2)}(k)\right)\Bigg] \\ &\quad +2\Bigg[\sum_{m_1=1}^{M-1}\sum_{m_2=m_1+1}^{M}\sum_{n=1}^{2}\left|G_{1,\mathrm{RX}(m_1)}(k)G_{1,\mathrm{RX}(m_2)}(k)\right. \\ &\qquad \left.\times\left(G^*_{1,\mathrm{TX}(n)}(k) + \frac{G^*_{2,\mathrm{TX}(n)}(k)s_p^*}{s_p}\right)\right|^2 \\ &\qquad \times\left(|G_{1,\mathrm{TX}(n)}(k)|^2 + |G_{2,\mathrm{TX}(n)}(k)|^2\right)\Bigg] \\ &\quad -(4M+2)\mathrm{Re}\Bigg[\sum_{m=1}^{M}\sum_{n=1}^{M}|G_{1,\mathrm{RX}(m)}(k)|^2 \\ &\qquad \times G_{1,\mathrm{TX}(n)}(k)\left(G^*_{1,\mathrm{TX}(n)}(k) + \frac{G^*_{2,\mathrm{TX}(n)}(k)s_p^*}{s_p}\right)\Bigg] \\ &\quad +(4M^2 + 2M)\end{aligned} \tag{A.3}$$

ACKNOWLEDGMENTS

This work was supported by the Academy of Finland (under Project no. 116423, "Understanding and Mitigation of Analog RF Impairments in Multiantenna Transmission Systems"), Tampere Graduate School in Information Science and Engineering (TISE), Nokia Foundation, HPY Foundation, and the Technology Industries of Finland Centennial Foundation, all of which are gratefully acknowledged. The authors would like to thank the anonymous reviewers for carefully reviewing the paper and for suggestions

and comments that helped us to improve the quality of the manuscript.

REFERENCES

[1] R. Tafazolli, Ed., *Technologies for the Wireless Future: Wireless World Research Forum (WWRF)*, Wiley, Chichester, UK, 2004.

[2] H.-H. Chen, M. Guizani, and J. F. Huber, "Multiple access technologies for B3G wireless communications," *IEEE Communications Magazine*, vol. 43, no. 2, pp. 65–67, 2005.

[3] A. Paulraj, R. Nabar, and D. Gore, *Introduction to Space-Time Wireless Communications*, Cambridge University Press, Cambridge, UK, 2003.

[4] D. Gesbert, M. Shafi, D.-S. Shiu, P. J. Smith, and A. Naguib, "From theory to practice: an overview of MIMO space-time coded wireless systems," *IEEE Journal on Selected Areas in Communications*, vol. 21, no. 3, pp. 281–302, 2003.

[5] S. M. Alamouti, "A simple transmit diversity technique for wireless communications," *IEEE Journal on Selected Areas in Communications*, vol. 16, no. 8, pp. 1451–1458, 1998.

[6] 3GPP Technical Specification Group Radio Access Network, "User equipment (UE) radio transmission and reception (FDD)," Technical Specification TS 25.101, v7.2.0, December 2005.

[7] 3GPP Technical Specification Group Radio Access Network, "Overall description of E-UTRA/E-UTRAN; stage 2," Tech. Rep. TR 36.300, March 2007.

[8] B. Razavi, *RF Microelectronics*, Prentice-Hall, Englewood Cliffs, NJ, USA, 1998.

[9] S. Mirabbasi and K. Martin, "Classical and modern receiver architectures," *IEEE Communications Magazine*, vol. 38, no. 11, pp. 132–139, 2000.

[10] M. Valkama, J. Pirskanen, and M. Renfors, "Signal processing challenges for applying software radio principles in future wireless terminals: an overview," *International Journal of Communication Systems*, vol. 15, no. 8, pp. 741–769, 2002.

[11] G. Fettweis, M. Lohning, D. Petrovic, M. Windisch, P. Zillmann, and W. Rave, "Dirty RF: a new paradigm," in *Proceedings of the IEEE International Symposium on Personal, Indoor and Mobile Radio Communications (PIMRC '05)*, vol. 4, pp. 2347–2355, Berlin, Germany, September 2005.

[12] J. Liu, "Impact of front-end effects on the performance of downlink OFDM-MIMO transmission," in *Proceedings of the IEEE Radio and Wireless Conference (RAWCON '04)*, pp. 159–162, Atlanta, Ga, USA, September 2004.

[13] R. M. Rao and B. Daneshrad, "I/Q mismatch cancellation for MIMO-OFDM systems," in *Proceedings of the IEEE International Symposium on Personal, Indoor, and Mobile Radio Communications (PIMRC '04)*, vol. 4, pp. 2710–2714, Berlin, Germany, September 2004.

[14] H. Kamata, K. Sakaguchi, and K. Araki, "An effective IQ imbalance compensation scheme for MIMO-OFDM communication system," in *Proceedings of the IEEE International Symposium on Personal, Indoor, and Mobile Radio Communications (PIMRC '05)*, vol. 1, pp. 181–185, Berlin, Germany, September 2005.

[15] M. Valkama, Y. Zou, and M. Renfors, "On I/Q imbalance effects in MIMO space-time coded transmission systems," in *Proceedings of the IEEE Radio and Wireless Symposium (RWS '06)*, pp. 223–226, San Diego, Calif, USA, January 2006.

[16] Y. Zou, M. Valkama, and M. Renfors, "Digital compensation of I/Q imbalance effects in space-time coded transmit diversity systems," to appear in *IEEE Transactions on Signal Processing*.

[17] Y. Zou, M. Valkama, and M. Renfors, "Performance analysis of space-time coded MIMO-OFDM systems under I/Q imbalance," in *Proceedings of the IEEE International Conference on Acoustics, Speech, and Signal Processing (ICASSP '07)*, vol. 3, pp. 341–344, Honolulu, Hawaii, USA, April 2007.

[18] R. M. Rao and B. Daneshrad, "Analog impairments in MIMO-OFDM systems," *IEEE Transactions on Wireless Communications*, vol. 5, no. 12, pp. 3382–3387, 2006.

[19] J. Crols and M. S. J. Steyaert, *CMOS Wireless Transceiver Design*, Kluwer Academic, Dordrecht, The Netherlands, 1997.

[20] A. Tarighat and A. H. Sayed, "MIMO OFDM receivers for systems with IQ imbalances," *IEEE Transactions on Signal Processing*, vol. 53, no. 9, pp. 3583–3596, 2005.

[21] A. Tarighat and A. H. Sayed, "Space-time coding in MISO-OFDM systems with implementation impairments," in *Proceedings of the IEEE Sensor Array and Multichannel Signal Processing Workshop (SAM '04)*, pp. 259–263, Barcelona, Spain, July 2004.

[22] T. C. W. Schenk, P. F. M. Smulders, and E. R. Fledderus, "Estimation and compensation of TX and RX IQ imbalance in OFDM-based MIMO systems," in *Proceedings of the IEEE Radio and Wireless Symposium (RWS '06)*, pp. 215–218, San Diego, Calif, USA, January 2006.

[23] Y. Tanabe, Y. Egashira, T. Aoki, and K. Sato, "Suitable MIMO-OFDM decoders to compensate IQ imbalance," in *Proceedings of the IEEE Wireless Communications, Networking Conference (WCNC '07)*, pp. 863–868, Hong Kong, March 2007.

[24] T. C. W. Schenk, P. F. M. Smulders, and E. R. Fledderus, "Estimation and compensation of frequency selective TX/RX IQ imbalance in MIMO OFDM systems," in *Proceedings of the IEEE International Conference Communications (ICC '06)*, pp. 251–256, Istanbul, Turkey, June 2006.

[25] P. J. Schreier and L. L. Scharf, "Second-order analysis of improper complex random vectors and processes," *IEEE Transactions on Signal Processing*, vol. 51, no. 3, pp. 714–725, 2003.

[26] T. B. Sorensen, P. E. Mogensen, and F. Frederiksen, "Extension of the ITU channel models for wideband (OFDM) systems," in *Proceedings of the IEEE Vehicular Technology Conference (VTC '05)*, pp. 392–396, Dallas, Tex, USA, September 2005.